2-8-2011

Nanoscale Carbon Architectures for Electrode Applications

Stephen Wakeland

Stephen Wakeland

Candidate

Mechanical Engineering

Department

This thesis is approved, and it is acceptable in quality and form for publication:

Approved by the Thesis Committee:

Dr. Claudia Luhrs, Chairperson

Dr. Zayd Leseman

Dr. Yu-Lin Shen

Dr. Bernie Carpenter

Dr. David Chapman

Accepted:

Dean, Graduate School

11/15/2010

Date

NANOSCALE CARBON ARCHITECTURES FOR ELECTRODE APPLICATIONS

BY

STEPHEN WAKELAND

PREVIOUS DEGREES
BACHELOR OF SCIENCE, MECHANICAL ENGINEERING
UNIVERSITY OF NEW MEXICO
SPRING 2009

THESIS

Submitted in Partial Fulfillment of the
Requirements for the Degree of

Master of Science in Mechanical Engineering

The University of New Mexico
Albuquerque, New Mexico

December 2010

DEDICATIONS

This work is dedicated to my wonderful family who were the first to teach me the importance of knowledge and for whose continued support I am ever grateful. This work is also dedicated to my girlfriend Eve Sieber whose love, support, and companionship I cherish.

Acknowledgements

I would like to thank everyone who contributed to this work. First and foremost, my advisor Dr. Claudia Luhrs from whom I've learned so much and who has been an excellent mentor, both as a thesis advisor and a research advisor. Also, Dr. Bernie Carpenter and Dr. David Chapman, with the Air Force Research Laboratory, who have been great collaborators with this research as well as excellent sources of knowledge. Ricardo Martinez whose assistance in the lab has been invaluable, and Timothy Labert of Sandia National Labs for providing BET measurements. I would also like to acknowledge Mike Majedi for his patience and generosity in providing me with the equipment I would otherwise not have had access to. Lastly, thank you to the committee members who accepted the task of reviewing this work, including Dr. Zayd Leseman and Dr. Yu-Lin Shen as well as Dr. Bernie Carpenter, Dr. David Chapman and Dr. Claudia Luhrs.

NANOSCALE CARBON ARCHITECTURES FOR ELECTRODE APPLICATIONS

BY

STEPHEN WAKELAND

ABSTRACT OF THESIS

Submitted in Partial Fulfillment of the
Requirements for the Degree of

Master of Science in Mechanical Engineering

The University of New Mexico
Albuquerque, New Mexico

December 2010

Nanoscale Carbon Architectures for Electrode Applications

By:

Stephen Wakeland

B.S., Mechanical Engineering, University of New Mexico, 2009

ABSTRACT

Two primary objectives were the basis of this research. The first objective was to synthesize a variety of carbonaceous nanomaterials using plasma torch and furnace-based expansion-reduction techniques. The second objective was to correlate the unique characteristics of these materials to their electrical properties when assembled into electrochemical double-layered capacitors (EDLCs), or supercapacitors.

A microwave atmospheric plasma torch was used to produce graphene and diverse graphitic and amorphous carbon nanomaterials. Direct high-temperature conversion under an argon plasma atmosphere of various hydrocarbons, in solid, liquid, and gaseous states, yielded carbon nanoparticles, nanoparticle/sheet mixtures, and graphene respectively.

Graphene was also produced using a novel furnace treatment consisting of a simple two-step process: Graphite oxide (GO) was mixed with an expansion–reduction agent (urea) that decomposed upon heating, releasing reducing gases. The mixture was then heated in an inert gas environment (N_2) for a very short time and moderate temperature (600 °C).

The morphologies of all products produced were studied using Transmission Electron Microscopy (TEM) and Scanning Electron Microscopy (SEM), while the crystalline structure and relative percentage of crystalline material was analyzed by X-ray Powder Diffraction (XRD) and Temperature Programmed Oxidation (TPO) methods. Thermogravimetric Analysis/Differential Scanning Calorimetry (TGA/DSC) was used to study the GO/urea mixture's decomposition-reduction process. Electron Energy Loss Spectroscopy (EELS) analysis of both samples produced using the torch and expansion-reduction methods is also presented. Characterization of the graphene samples was also performed using Raman Spectroscopy. The samples surface area and functional groups were also analyzed using BET, and point-of-zero-charge (PZC) analysis respectively.

The materials produced were formed into thin-film electrodes and their capacitances and resistances were evaluated. The electrical data recorded for each material as well as the characterization of their structure was used to correlate microstructural characteristics of each material to its electrical properties as an EDLC electrode material.

This work exemplifies the usefulness of the plasma torch system as a means to generate diverse material architectures difficult to obtain by alternative routes, as well as the effectiveness and value of a new expansion-reduction process in producing graphene. This study also helps to shed light on some of

the mechanisms and characteristics of carbonaceous materials that contribute to their usefulness as functional materials in EDLCs.

TABLE OF CONTENTS

List of Figures

Chapter 3

Chapter 4

List of Tables

Chapter 1
Introduction and Background

As research efforts are increasingly focused upon renewable and efficient methods of energy production, major hurdles still remain regarding the effective and practical storage of the energy produced. Renewable energy resources, such as wind and solar, present clean alternatives to fossil fuels, although they require the use of devices, such as batteries and supercapacitors, to store harvested energy in a manner that allows the energy to be supplied without major interruptions or fluctuations. Similar requirements are required for transportable electronic equipment and components such as remote sensors or satellites.

1.1 Defining Supercapacitors

Traditional forms of energy storage include batteries and capacitors. Batteries utilize Faradaic reactions (electrochemical) to store energy and release it upon discharging. They have excellent energy densities but low power densities, when compared to capacitors. Also, the phase changes of chemicals between the anode and cathode produce a slight irreversibility, which in turn diminishes the battery's cycle life.

In contrast, capacitors store energy through non-Faradaic, electrostatic mechanisms. There are no chemical changes in a traditional capacitor; a charge builds up simply as an excess and deficiency of electrons on the surface of two plates, separated by a dielectric. Because capacitors do not require any

chemical interactions to store or move charge, they have superb cycle lives and excellent power densities. However, their energy density is very low compared to batteries, which limits the potential use of capacitors. Supercapacitors or electric double-layer capacitors (EDLC) are designed to bridge the gap between batteries and capacitors. They have improved energy densities resulting from double layers of charged electrode/electrolyte interfaces, yet still maintain excellent cycle lives and power densities. Because the energy density of a supercapacitor depends on the area on which electrode/electrolyte interactions can occur, materials with high surface areas are essential. Researchers have turned to nanomaterials to further increase electrode surface area, and in turn, capacitance. Figure 1.1 illustrates the differences between a traditional capacitor and a supercapacitor.

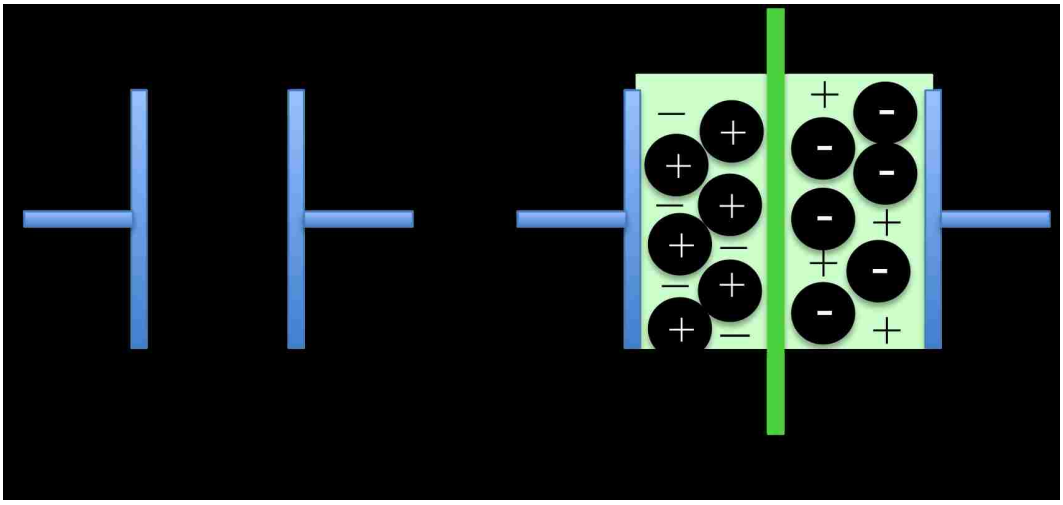

Figure 1.1: Basic schematic of an electrostaic capacitor (left) and an electrochemical double-layer capacitor (right).

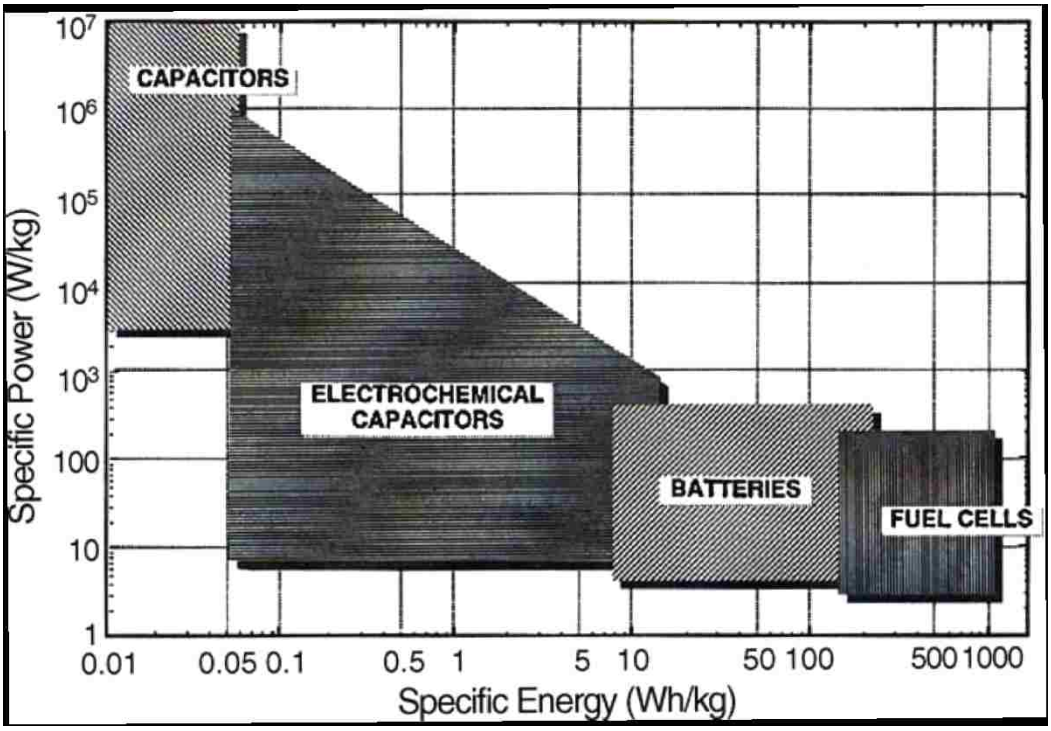

Figure 1.2: Specific energy and power capabilities of fuel cells, batteries, electrochemical capacitors (supercapacitors), and capacitors (electrostatic) [1]

Figure 1.2 shows the specific energy and power capabilities of several of the most common energy storage devices. The power and energy storage capabilities of batteries and capacitors are closely associated with the physical and chemical characteristics of their electrodes. At present, optimization of the carbon electrodes is needed in order to maximize electric performance as a function of porosity, surface functionality, wettability, and reductions in inter-particle contact resistance. This work was designed to address some of the issues related to optimization of electrode materials by generating carbonaceous products with a range of characteristics and determining which characteristics contribute to improved performance. In addition to contributing to existing studies

on surface area, [2, 3] this thesis will examine for the first time, how the amount of crystalline material affects the capacitive properties of a carbonaceous material.

1.2 Thesis Outline

This manuscript is organized into several chapters: Chapter 1 outlines the thesis content and composition and introduces the concepts and principles of supercapacitors, as well as theories behind current research trends. The various carbonaceous materials studied during this endeavor are also introduced.

Chapter 2 discusses the synthesis and characterization of all the carbonaceous materials synthesized using plasma torch methods. The aerosol microwave plasma approach provides unique product features. Our research group has become a leader in its operation and the generation of products difficult to obtain by alternative routes. Chapter 2 describes the aerosol-through-plasma method of synthesis, the analysis techniques used to characterize the samples, and an in-depth discussion of the unique morphology of each sample.

Chapter 3 presents the novel expansion-reduction technique, developed by our group, that produces graphene under moderate temperatures and easily scalable operating conditions. The urea mediated expansion-reduction process is described in depth, as well as the necessary steps required for this unique method of synthesis. The characterization techniques and morphology of the samples are discussed as well. Chapters 2 and 3 are directly based on articles

previously published by our group [4, 5]. The materials discussed in these chapters were further analyzed and characterized after their corresponding articles were published. As a result, this additional work is discussed further in Chapter 4. Chapter 4 also describes in detail the methods used to evaluate the capacitance of each material. The capacitance measurements and the correlations between microstructure and capacitance are presented in Chapter 5. Finally, in Chapter 6, conclusions are drawn and future work is also suggested.

1.3 Previous Work in the Field of Supercapacitors

Within the last two decades, carbon materials have generated a renewed interest in the scientific community, as new materials are being introduced, and new applications for these materials, as well as more traditional forms of carbon, are developed. A noticeable increase in battery and EDLC performance is an exciting and significant example of the result of using carbon nanomaterials. One of the recent additions to the list with carbon materials of technological promise is graphene. The potential applications proposed for graphene arise from several unique features: the mechanical strength inherent in the strong covalent bond between adjoining carbon atoms in a basal plane, the potential to organize graphene to create 'molecular scale' circuit elements, and the unique chemistry of the 'edges' of a graphene sheet. Graphene is best described as a sheet (or no more than a few stacked sheets) of hexagonally bonded carbon atoms. Graphene may be envisioned as an infinite, two-dimensional molecule. The

larger, three-dimensional structure of basal graphite is composed of a multitude of graphene sheets. Figure 1.3 illustrates the differences between graphene and graphite.

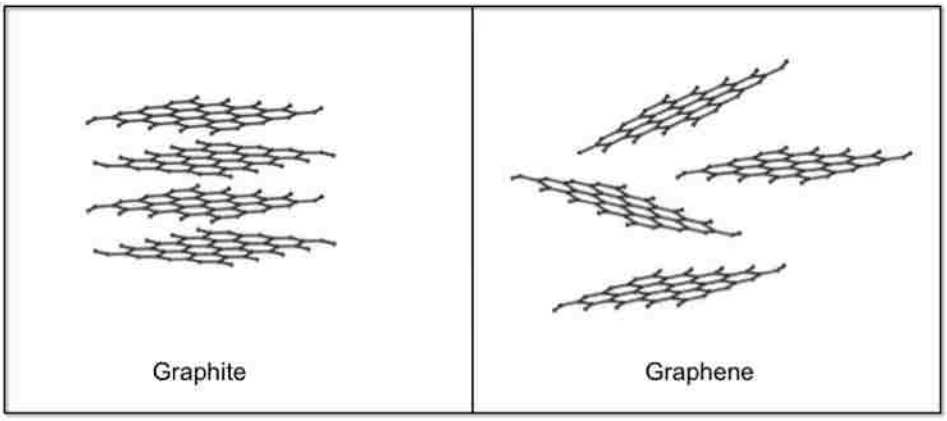

Figure 1.3: Molecular representation of graphite (left) and graphene (right)

Examples of recently proposed applications that use all or some of the properties of graphene are outlined next. Due to the changes in structural and electronic properties observed in graphene when it absorbs molecules, it can be used as gas and biosensors, either as pristine, B- or N-doped [6-8]. Graphene also exhibits potential for use as resonator materials as a result of graphene's thermal conductivity, mechanical properties such as strength and stiffness, and its tunable electrical properties [9]. Composites are yet another potential application of graphene. Graphene dispersed in polymer may find uses as filler material for reinforcements or conductive polymer generation [10-12]. Composites made from electro spun polymer nanofibers containing graphene nanoplatelets have shown improved Young's moduli [13]. A recent publication highlights the use of graphene in dual gate FETs [14], adding to the list of

proposed applications of graphene for use in the electronics industry [15-17]. Graphene has also been targeted for supercapacitor electrodes due to its high electrical conductivity, which improves performance over a wider range of voltage scan rates [18]. Battery, fuel cell and solar cell components based on graphene are an example of how this material is finding use in multiple energy related applications, including both energy generation and storage [14, 18-22]. More traditional materials, such as carbon fibers and activated carbons, also have been used as electrode materials in devices related to energy storage applications [2, 3, 23-25].

Multiple processes for the production of graphene and graphitic like sheets and particles have been reported; chemical vapor deposition (CVD) and related methods that generate free standing graphene sheets [26, 27], thermal exfoliation of graphite oxide [28-30], and wet chemistry reduction techniques that employ graphite oxide as precursor and reducing agents such as hydrazine or urea and additives to eliminate oxygen groups [5, 12, 31, 32] are some examples. Carbon nanoparticles also can be produced using carbonization processes. These processes make use of different organic compounds as precursors [33].

1.4 Justification for this Study

Each synthetic method creates materials with unique characteristics. The dependence of the microstructural characteristics of the produced material on the

type of synthesis is one of the primary justifications for this research endeavor. Our work began with synthesizing a variety of carbonaceous materials using the plasma torch and urea expansion-reduction methods, and the evaluation of their microstructural qualities such as crystallinity, surface area, and surface functional groups present. These materials include amorphous and graphitic carbon nanostructures (both particles and sheets) as well as graphene. The differences between these materials begin with the diverse hydrocarbons that are the source of each synthesized material. Materials synthesized through the plasma torch procedure are derived from precursors such as solid anthracene, liquid hexane, and ethylene gas. The graphene sheets produced using the novel furnace treatment, developed by our group, begin as a mixture of graphite oxide (GO) and urea. For ease of clarification throughout this manuscript, the carbonaceous materials synthesized from ethylene, hexane and urea are named by their precursor material or method (i.e. graphene samples made from urea methods are named simply samples from urea).

The other main justification of this work was that we would correlate the qualities of each material to some of their electrical properties. We achieved this by forming electrode films from each carbonaceous material and assembling the electrodes into EDLC test cells. With multiple test cells for each material (except for the ethylene-generated graphene as a result of low production yields), the electrical properties were evaluated using a National Instruments Educational Laboratory Virtual Instrumentation Suite (ELVIS) testing board. The ELVIS

testing method allowed us to measure both the total capacitance as well as total resistance of each cell. These values as well as the data collected from the ELVIS unit give an excellent quantitative idea of how the microstructure of carbon materials affect their electrical properties.

1.5 Thesis Hypotheses

The main concepts driving this research are described succinctly by the following three hypotheses:

Hypothesis 1: Through careful selection of operational parameters of the plasma torch synthesis process, we will be able to generate solid carbonaceous nanostructures with high surface areas, high levels of graphitization, and nanoscale dimensions.

Hypothesis 2: A hydrocarbon that produces reducing gases upon decomposition will simultaneously exfoliate and reduce graphite oxide, yielding graphene sheets.

Hypothesis 3: The aerosol-through-plasma and expansion-reduction synthesis processes generate carbonaceous nanomaterials that can be used as electrode material in supercapacitor devices.

In all, this study provides evidence on how the microwave plasma approach as well as the furnace treatment involving urea can be used as alternative routes to generate carbon electrode architectures with highly controlled morphologies and varying degrees of graphitization. The information garnered through the testing involved in this research also elucidates some of the dependencies of electrical properties on material microstructure.

Chapter 2
Synthesis of Electrode Materials Through Novel Plasma Torch Methods

2.1 Experimental Procedures of Plasma Torch Synthesis

Microwave plasma synthesis of various carbon nanomaterials was performed using an Astex microwave plasma generator operating at 900 Watts at approximately atmospheric pressure. Argon was used as plasma gas with flow rates of 3.5 slpm. The basic configuration of the system can be observed in Figure 2.1. In this technique, the solid, liquid or gas that serves as a precursor material is carried along by a gas as an aerosol (Point A) through an atmospheric pressure microwave plasma (Point B) that converts it into more valuable product (nanoparticles / graphene sheets) which then passes through a chimney in the afterglow region (Point C) before being collected by a filter system (Point D). The red arrows indicate the flow of the precursor and the resulting carbon material.

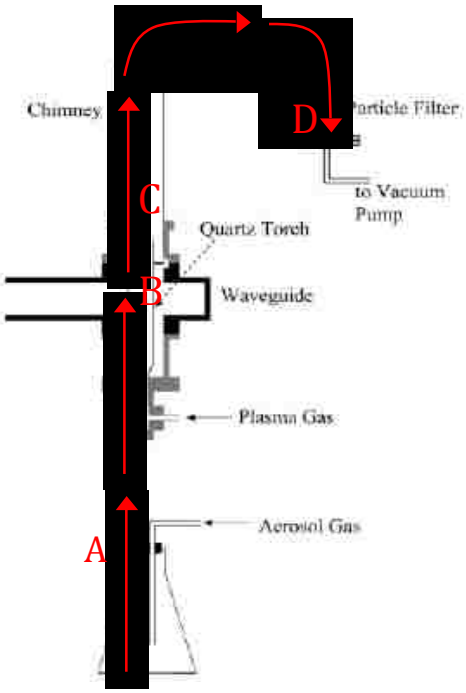

Figure 2.1 Aerosol-through-plasma system diagram

2.1.1 Solid Precursor: Anthracene

500 mg of finely ground commercial anthracene (Sigma Aldrich, reagent grade) were placed in a beaker to be used as a carbon source, see Figure 2.2 for the chemical structure. The container with anthracene was then attached to 2 lines; one inlet introduced Argon gas (UHP) into the beaker. This gas functioned as the aerosol or carrier gas. The flow rate for this gas varied between 0.3 to 1.1 slpm. The slower flowrate was used to create the graphitic nanoparticles while the faster yielded amorphous nanoparticles. A slower flow rate will provide the particles with more residence time in the hot zone of the plasma, increasing graphitization. The other line was the outlet and was connected the beaker to an alumina tube. To aid the particles' vibration and their incorporation into the aerosol or carrier gas stream, the beaker containing the solid precursor was placed inside an ultrasonic bath. Together, the solid precursor and the gas formed an aerosol that was fed, through the alumina tube, to the center of the discharge zone of the plasma. Although the experiments were carried out in conditions considered to be atmospheric pressure, a tight regulation of the exhaust pressure (0.013 atm above atmospheric) was maintained.

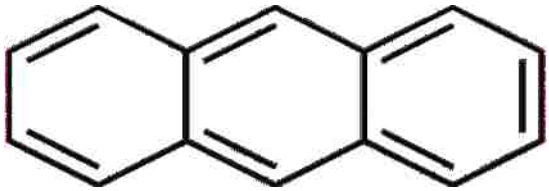

Figure 2.2: Chemical structure of anthracene.

2.1.2 Liquid Precursor: n-Hexane

A slight modification of the system's precursor inlet was required in order to use a liquid precursor: n-hexane (EMD High purity). Two beakers, one containing the liquid, and one serving as a trap, replaced the beaker from Figure 2.1 (Point A). The use of a liquid precursor made it unnecessary to use an ultrasonic bath. The second beaker, or trap, was used to keep liquid from directly entering into the plasma discharge zone in the event of a negative pressure condition. Aerosol gas (Ar, UHP) was directed at the surface of the liquid to generate the aerosol vapor. An extra Ar gas flow was inserted in the second trap in order to further dilute the n-hexane vapor before entering the alumina tube that connected these reservoirs with the plasma hot zone. The rest of the system, including afterglow and collection filter, remain unmodified.

2.1.3 Gas Precursor: Ethylene

For the introduction of gas precursor into the plasma system only one line was employed to connect the carbon source and the alumina tube. It was fed by a T-tube that mixed ethylene (Matheson Tri gas, 1% dilution in UHP Argon) and an extra Ar gas line for further dilution. No ultrasonic bath or traps were used.

2.2 Samples Characterization

TEM and EELS samples characterization were conducted on a JEOL 2010 high resolution transmission electron microscope (HRTEM) and JEOL 2010F FASTEM field emission gun scanning transmission electron microscope (STEM/TEM) equipped with a Gatan GIF image filtering system for energy filtered TEM and EELS analysis. SEM analysis was performed on a Hitachi S-5200 Nano SEM working at 2-10 kV.

Samples also were analyzed using a Scintag Pad V diffractometer / goniometer with scintillation detector, Datascan software (Materials Data, Inc.) for diffractometer automation - data collection, and Jade Software (Versions 9, also from MDI) for data analysis. Temperature Programmed Oxidation (TPO) analysis of the samples were carried out in a Netzch STA 409, in which the samples' burn off processes were studied under 95%/5% N_2/O_2 atmospheres (60 ml/min) with heating rates of 5 °C/min from room temperature to 900 ^oC.

2.3 Results and Discussion

It is widely known that plasma discharges can modify materials surfaces and their properties. This phenomenon is the foundation of processing technologies of pivotal importance for today's manufacturing industry. Large-scale production of integrated circuits for the electronic industry is the most widely known example of plasma discharge application. Plasma processes also are indispensable in the aerospace, automotive, steel, solar and biomedical

industries, and produce material surface characteristics that would be difficult to obtain by alternative methods.

Commercially available plasma-related methods include materials deposition, removal, patterning and modification of electrical properties. Plasma techniques based on argon or oxygen discharges are responsible for the generation of Al, W and superconducting films, while oxygen discharges have been utilized to grow Si, Si_3N_4 and SiO_2 films. Boron halide discharges are used for B implantation in silicon and diverse compositions (i.e. CF_4, O_2, Cl_2) used to selectively remove silicon films [34]. Oxygen discharges also can remove photoresist and activate diverse surfaces, even promote polymerization processes. For the microfabrication of an integrated circuit a considerable number of steps involve some type of plasma-based technology.

In contrast with thin film fabrication techniques, the approaches used to generate particulate and free-standing materials are not usually focused on plasma methods. Apart from the creation of islands and clusters by sputtering techniques, which usually are grown to eventually form extended films, plasma based methods have also found a niche in the thin film technology industry by providing an alternative to other techniques, such as ones based on colloids, micro-emulsions and sol gel approaches, for the generation of particles and stand-alone sheets. To our knowledge, only a few examples in the literature focus on the production of either isolated carbon particles, secluded sheets or fibers by using atmospheric microwave plasma approaches: those conducted by

Phillips et al. and Dato et al. [35, 36].

Our work extends the scope of previous efforts in the field by using hydrocarbons in different states (solid, liquid and gas) to produce carbon nanostructures using an atmospheric plasma system. We also attempted to modify process variables in order to induce different levels of graphitization in the products. Because no catalyst particles were employed, we expected to generate non-fibrous samples. The selection of the solid hydrocarbons was made on the basis of previous knowledge regarding the feasibility to graphitize the selected precursor. Given that the degree of graphitization of a carbon precursor depends on the characteristics of the product of carbonization (if it forms a coke or a char), we used coke-forming precursors. Anthracene consists of three benzene rings. It is a planar molecule well known to form coke once it loses its hydrogen atoms, and a free radical mechanism induces the condensation of larger planar molecules. Coke-forming precursors, usually with linear coplanar structures, will readily graphitize after the carbonization temperature is reached. In contrast, char forming precursors, usually with branched structures, will not form extensive graphitic structures but form random arrangements of crystallites.

We observed that, from the experimental conditions that can be controlled (such as flow rates in aerosol and plasma gas, generator power and exhaust pressure), aerosol flow rates seem to have the greatest influence on the products' microstructural features when solid anthracene was used as carbon precursor. High aerosol (argon gas with anthracene particles suspended on it)

flow rates promoted a rapid carbonization processes, in which anthracene passed through the discharge zone and rapidly transformed to produce a black solid composed by spherical nanoparticles with an average size between 11-15 nm (Figure 2.3a).

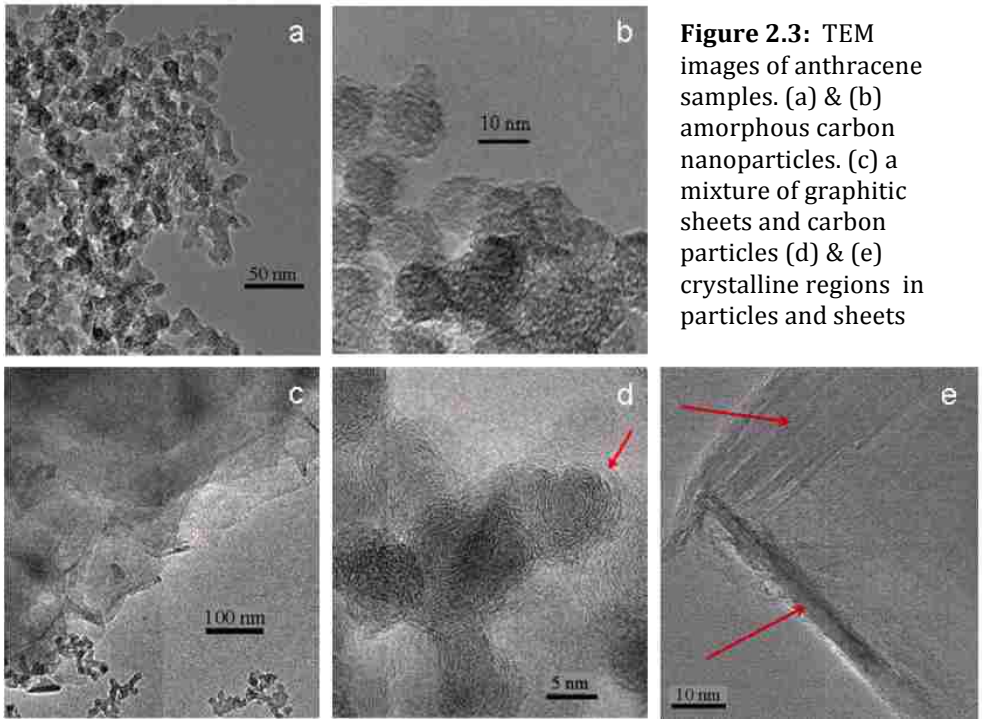

Figure 2.3: TEM images of anthracene samples. (a) & (b) amorphous carbon nanoparticles. (c) a mixture of graphitic sheets and carbon particles (d) & (e) crystalline regions in particles and sheets

HRTEM studies of the particles showed turbostratic material characteristics, with no evidence of long-range order in the particles (2.3b). When the synthesis conditions were changed and the particles were forced to have longer residence times in the hot zone of the system (by changing aerosol gas flow rates from 1.1 slpm to 0.3 slpm), a drastic change in the sample microstructure was observed: carbon deposits were no longer composed exclusively of nanoparticles but included carbon sheets that extended for hundreds of nanometers, reaching in

occasions lengths in the order of microns (2.3c). Moreover, the spherical particles contained in such samples presented concentric lattice fringes with spaces between 0.33-0.34 nm, typical of graphitic substances (2.3d). Extended carbon sheets in the sample clearly presented crystalline characteristics (2.3e).

It has long been stated that the use of pressure can enhance the graphitization process and shorten heat treatment times [37]. In our case, a variation in process conditions to allow longer residence times (still in the order of milliseconds) is observed to have similar effects. The advantage of controlling residence times instead of increasing system pressure is that the yields are not heavily impacted with the change in flow rates, while changes in pressure noticeably decrease yields.

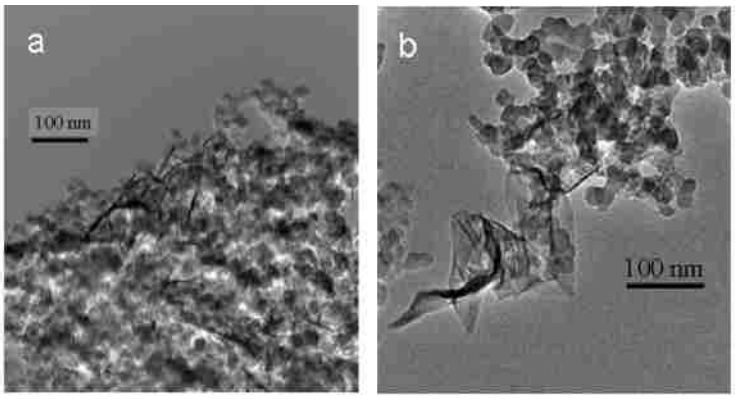

Figure 2.4: TEM images of samples produced from hexane. (a) carbon products generated by plasma treatment of liquid hexane yield mainly amorphous nanoparticles. Thin carbon sheets are sometimes found mixed with particles. (b) lengths of sheets were found to be within a few hundred nm

The use of n-hexane as precursor in the conditions described in section 2.1 renders samples that (regardless the flow rates employed) present both carbon particles and sheets (Figure 2.4a and b). None of these features present

long-range order characteristics. Sheets seem shorter than the ones observed for anthracene, in the order of few hundred nanometers. Sheet thickness, although not measured, always appeared thinner when hexane is employed as precursor.

Ethylene has been used as feedstock material to produce carbon fibers and nanotubes [38, 39] by flame and related methods. In the present work, ethylene was fed into the microwave plasma system after dilution with argon. The samples generated present graphene-like characteristics: they consist of extended carbon films. No particles were observed. The films formed entangled sheets or crumpled spherical agglomerates depending on the zone of the system in which they were collected. In all cases, careful sample preparation for TEM observation using solvents helped collect flat sheets. See Figure 2.5. SEM images (2.5b and c) show that aggregates collected in the quartz tube located in the system coupler region are on the order of 500 nm. The yields of carbonaceous product generated from this gas precursor are 1/10 to 1/20 the weight of materials prepared from solid precursors for a given run time. Samples produced from ethylene present lattice fringes when studied by HRTEM (figure not shown).

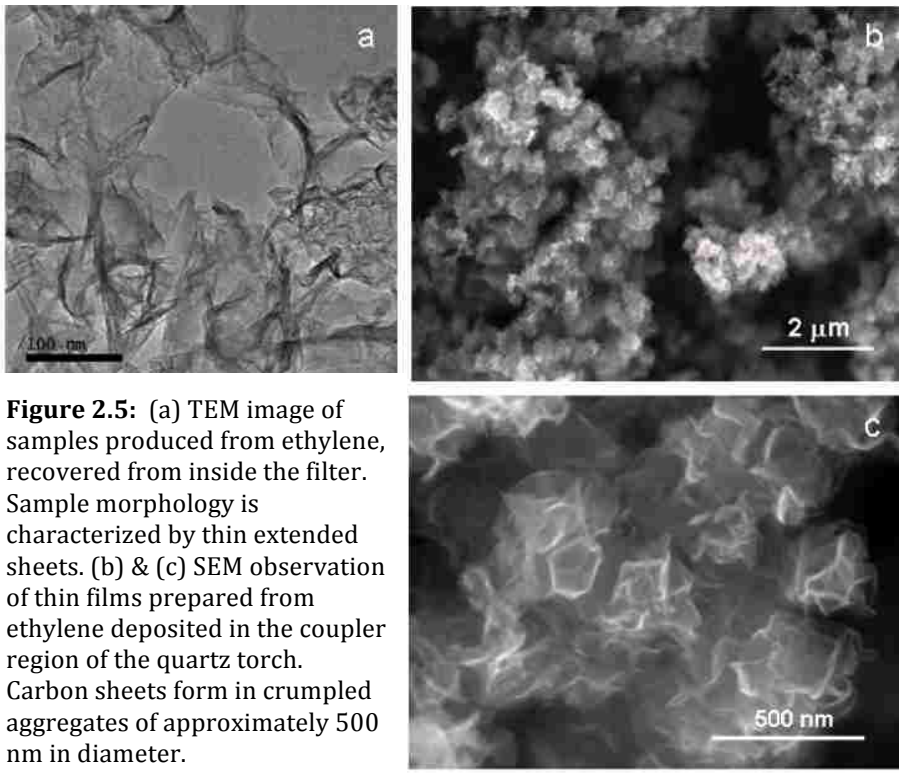

Figure 2.5: (a) TEM image of samples produced from ethylene, recovered from inside the filter. Sample morphology is characterized by thin extended sheets. (b) & (c) SEM observation of thin films prepared from ethylene deposited in the coupler region of the quartz torch. Carbon sheets form in crumpled aggregates of approximately 500 nm in diameter.

Carbon samples originating from the previously mentioned precursors were studied using thermogravimetric analysis techniques. In particular, temperature programmed oxidation studies were performed in atmospheres containing 5% O_2 in N_2, and at heating rates of 5 °C/min. Previous TPO studies of similar carbon-based samples have shown that amorphous carbon oxidizes at lower temperatures than graphitic carbon [40]. With this knowledge and the data we collected, it was then possible to make assumptions regarding the crystalline components of the materials based on their oxidation temperatures. We measured the oxidation process onset temperatures (in wt% vs. temperature) for

each plasma-produced sample (Figure 2.6). The values obtained demonstrate a dependence based on the type of precursor used and changes in synthesis conditions, as in the case of anthracene-based samples. The level of graphitization in samples follows the scheme:

graphene from ethylene > graphitic particles from anthracene > amorphous particles from anthracene > particle-sheet mixtures produced from hexane. The temperature onsets are 705> 592 > 581 > 519 °C, respectively. The onsets were affected by a number of microstructural characteristics, such as particle size, as well as the level of graphitization. Each type of material onset temperature was determined by Netzch's analysis software, Proteus.

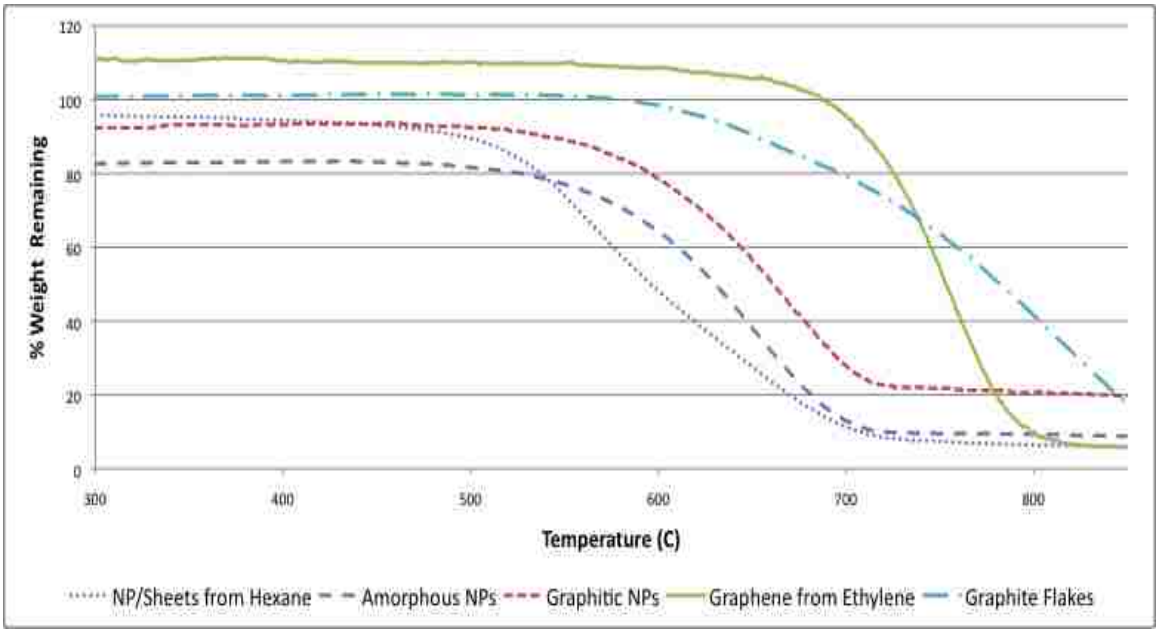

Figure 2.6: TPO analysis of the carbon samples shows that the burn off process temperature onset varies with precursor nature and condition of generation.

The temperature program oxidation curve of graphite flakes, (graphite flakes being the carbon material with the highest crystalline content available in our lab) is included in Figure 2.6 for comparison. This data shows that graphene from ethylene is the most graphitic sample as it follows the oxidation trend of graphite with burn off temperatures above 650 °C. In other words, samples generated from ethylene seem to have a larger component of graphitic structures when compared to those prepared from n-hexane. The onset temperature observed for graphene oxidation (above 700 °C) is very close to the one determined for the graphite sample (725 °C). Graphene sheets seemed to reach total oxidation values within shorter times than graphite flakes. We believe such differences are a result of graphene having more exposed surface area than graphite flakes, causing the graphene to react promptly.

Using hexane and anthracene as precursors seemed to generate carbon structures that still contained small amounts of the original material (precursor did not convert or react). TPO curves show that a small percentage of the sample's weight was lost at temperatures normally associated with the decompostition of organic compounds (close to 200 °C). Thus we can assume a small amount of anthracene remained in the amorphous and graphitic nanoparticles, and that the final products from hexane were slightly wetted with un-reacted hexane. Amorphous particles from anthracene (produced using higher aerosol flow rates for aerosol) seemed to have the larger amount of precursor in the product because the precursor spent less time in the hot zone of the plasma.

XRD analysis of the samples, performed at indentical scan rates, support the TPO data findings; ethylene used as a precursor renders more crystalline samples than its solid and liquid counterparts, evidenced by the higher intensity of the peak located close to 26° (2θ) of the X-ray diffraction pattern, which normally is associated with graphite and graphitic structures (Figure 2.7). The x-ray patterns of samples produced from anthracene contain peaks close to 26° but also present a sharp peak that was identified as anthracene. XRD analysis of all samples were analyzed at the same scan rate.

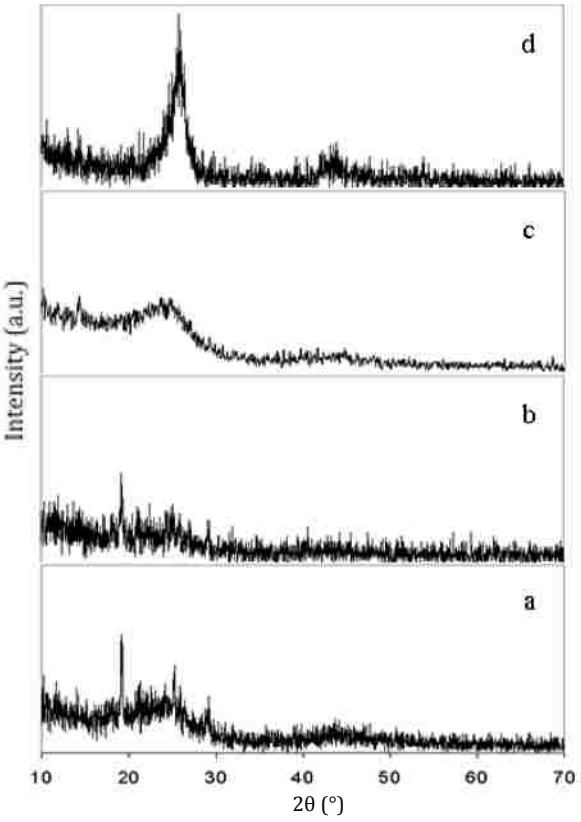

Figure 2.7: XRD patterns of carbon products. (a) graphitic nanoparticles generated from anthracene (b) amorphous nanoparticles generated from anthracene (c) product generated from hexane and (d) sheets generated from ethylene

The carbon nanostructures generated by the microwave plasma approach were analyzed by EELS to identify the characteristic graphitic related π* and σ* absorption peaks in the spectra (Figure 2.8). Those results also correlate with the XRD and TPO findings: samples prepared from ethylene (graphene sheets) and those in which TEM observations confirmed the presence of graphitic products, synthesized from anthracene at low flow rates (graphitic sheets and particles), have similar spectra, with maximums close to 285 and 292 eV as in other reported graphitic samples [41]. The samples generated from n-hexane do not show the 292 eV peak.

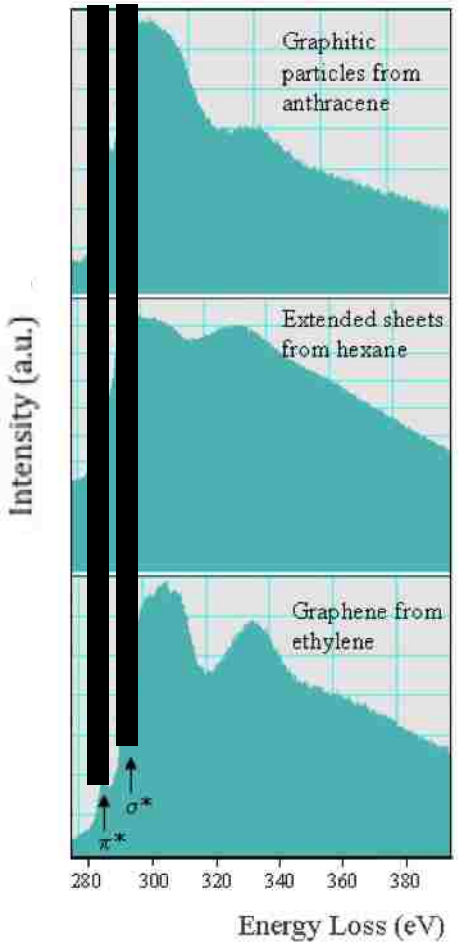

Figure 2.8: EELS analysis of carbon nanostructures produced by plasma methods

2.4 Summary of Torch Methods

The information presented in Chapter 2 shows that by altering the operating parameters of an atmosphere microwave plasma system we were able to synthesize a wide variety of carbonaceous nanostructures including amorphous and graphic nanoparticles (average size of <16nm), graphene, and mixtures of nanoparticles and graphitic sheets. System variables included the precursors, gas flow rates, and system pressure. Benefits of these types of synthesis include single-step synthesis (from precursor to end product), carbon materials with minimal surface groups, and tight control over levels of graphitization.

Chapter 3
Generation and Characterization of Graphene Utilizing Urea as an Expansion-Reduction Agent

3.1 Introduction to Expansion-Reduction Synthesis

Multiple processes have been reported for graphene production; CVD and related methods that generate graphene free standing sheets [26, 27], thermal exfoliation of graphite oxide [28-30], and wet chemistry reduction techniques that employ graphite oxide as precursor and reducing agents such as hydrazine and additives to eliminate oxygen groups [31, 32, 42-45]. It appears that each method creates graphene with unique characteristics. In the present manuscript we introduce a novel approach of generating graphene from graphite oxide. Unlike the common colloid approaches to reduce graphite oxide, we have used only solid precursors, moderate temperatures and urea as an expansion–reducing agent for graphene generation. This process is based on the hypothesis that the use of an expansion–reducing agent will: (a) promote an expansion of the graphite oxide layers at temperatures at which the agent (urea in this case) decomposes and produces volatile materials; and (b) because the byproducts of urea decomposition are reducing agents, the processes will allow the reduction of the oxygen-containing groups in the graphite oxide.

3.2 Experimental Procedures of Expansion-Reduction Synthesis

3.2.1 Graphite oxide (GO)

We followed the Hummers approach to produce graphite oxide [46]. The graphite oxide (GO) generation included the use of graphite flakes (Sigma–Aldrich), sulfuric acid (EMD), potassium permanganate (J.T. Baker), sodium nitrate (EMD) and hydrogen peroxide (EMD) followed by the typical hydrolysis, washing with DI water and drying steps, carefully controlling temperature through the entire process.

3.2.2 Graphene Preparation

Graphite oxide, prepared as outlined above, and urea (Sigma–Aldrich) were mixed as solids and ground in an agate mortar. GO/urea molar ratios of 1:1 and 1:2 were used. The GO/urea mixture was placed in a ceramic boat and introduced into a quartz tube of a tubular furnace. N_2 (UHP) gas flowed at 105 sccm during the full duration of the thermal treatment. The furnace (Lindberg Blue from Thermo Scientific) temperature was raised to the reaction temperature, 600 °C. We also employed reaction temperatures of 800 °C for comparison. The first temperature was selected because urea thermal decomposition occurs below 600 °C [47, 48]. The second temperature, 800 °C was selected to study higher temperature effects on the product. Reaction times were varied between 5 and 30 min. After the reaction temperature and dwell times were reached, power to the heaters was turned off, and the sample was allowed to cool to room

temperature.

An alternative pathway to the method described above was also used and consisted of heating the tubular furnace to the reaction temperature while the sample, a mixture of graphene oxide and urea, was placed in a ceramic boat inside a quartz tube with a N_2 flow of 105 sccm while the tube was still outside the furnace. Once the reaction temperature was reached, the tube (with sample inside) was placed inside the furnace for five minutes. The sample was then retrieved and left to cool.

A third variation to the protocol regarding how the GO and urea could be mixed was also be employed: combine GO with urea solutions (same molar ratios but adding water–ethanol to dissolve urea first) and then freeze dry the mixture before performing heat treatment.

3.3 Sample characterization

Samples were analyzed using a Scintag Pad V diffractometer/ goniometer with Scintillation detector, Datascan software (Materials Data, Inc.) for diffractometer automation – data collection, and Jade Software (Versions 9, also from MDI) for data analysis. TEM and EELS Characterization were performed on a JEOL 2010 high resolution transmission electron microscope (HRTEM) and JEOL 2010F FASTEM field emission gun scanning transmission electron microscope (STEM/TEM) equipped with Gatan GIF image filtering system for energy filtered TEM and EELS analysis. SEM analysis was conducted on a

Hitachi S-5200 Nano SEM working at 10 kV. TGA/DSC analysis was carried out in a Netzch STA 409, in which GO/urea mixtures, graphite flakes/urea mixtures and urea were studied under N_2 atmospheres with heating rates of 5 °C/min.

Nitrogen content of the samples was measured using a Elemental Analyzer coupled to a ThermoQuest Delta Plus Mass Spectrometer and oxygen percentage determined using a Thermo- Chemical Elemental Analyzer coupled to a Finnigan 252 Mass Spectrometer. Preliminary Raman data was acquired using a CCD Spectrograph single stage with 488 nm excitation.

3.4 Results and Discussion

3.4.1 Graphene Generation

Treating samples composed of graphite oxide and urea in inert atmospheres (i.e. N_2) above the urea decomposition temperature led to both a significant volume expansion and chemical reduction. The volumetric change occurred as the urea decomposes and volatile material from the same caused an exfoliation effect in the graphite oxide layers. The volume expansion was apparent to the naked eye when the cooled sample was retrieved from the furnace. SEM and TEM observations of the product corroborate that the process was not only evident at the macroscopic level but produced an exfoliation of layers on the nanoscale level. The graphite oxide reduction process (elimination of oxygen species in graphite oxide to render graphene) happened simultaneously, aided by the temperature employed and the reducing nature of

urea's decomposition products. The reduction process was substantiated by XRD analysis of the product and by the study of the reaction by thermogravimetric analysis. EELS examination of product confirmed the regeneration of a sp2 graphitic structure after the urea reaction with graphite oxide. The reduction mechanism will be reviewed and discussed in more detail in a subsequent section.

Figure 3.1 presents a comparison between the XRD reflections observed for graphite oxide (a) and graphene sample (b). The graphite oxide peaks included the characteristic reflection close to 12.6° and were also observed at approximately 26° and 43°. For graphene, the product of the reaction of graphite oxide and urea mixtures (1:1 M ratio) treated at 600 °C, XRD analysis did not show any remnant of the peak at lower angles, although peaks at approximately 26° and 43°, which is typical of graphitic substances, remain. The Raman spectra of carbon materials usually display a strong line (G) close to 1582 cm^{-1} and a line (D) around 1350 cm^{-1} [45]. Multiple factors, such as defects, doping and layer numbers can affect the position of the G band [49, 50]. In graphene sheets, the Raman spectra typically show a broadening and upward shift of the G band, while the intensity of the D line increases. Preliminary Raman spectra of a graphene sample produced by urea expansion–reduction process presents the characteristics expected from a graphene specimen, with G lines between 1586 and 1598 cm^{-1}, depending in the area analyzed. The D lines suffer an increase in intensity and are located between 1364 and 1367 cm^{-1}. The spectral window

range used for this preliminary analysis was too small to allow the acquisition of the bands near 2700 cm^{-1}, usually correlated to the graphene layer count [26, 45].

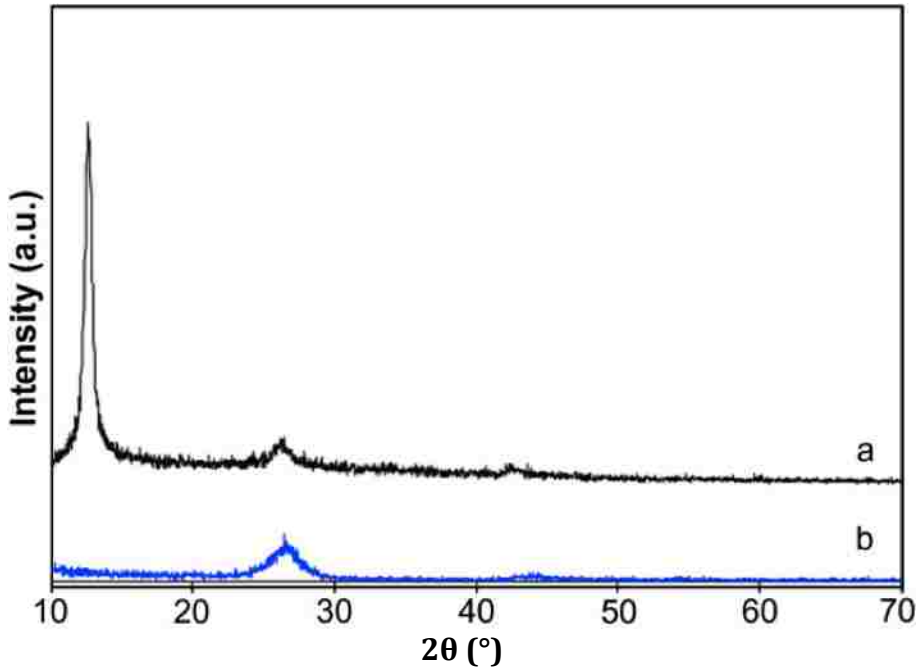

Figure 3.1: XRD analysis of (a) graphite oxide and (b) graphene – sample generated by urea based expansion-reduction treatment

Figure 3.2 illustrates the expansion and reduction process undergone by the GO, mediated by urea. In Figure 3.3, SEM observation of sample after urea treatment reveals the existence of very thin extended films that curve and reach tens of microns in length. Higher SEM magnification images of the sample show that in some regions graphene sheets are somewhat entangled, however, they still consist of extremely thin layers.

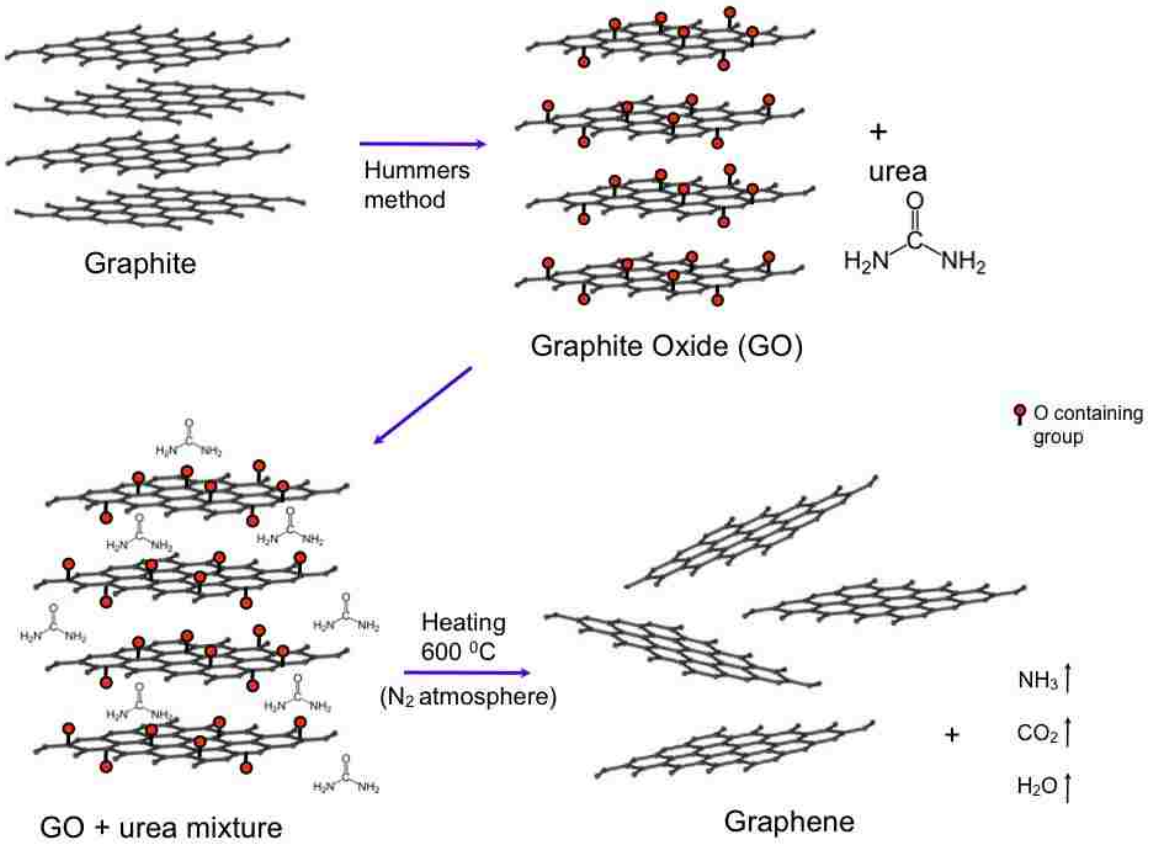

Figure 3.2: Illustration of expansion-reduction process beginning with graphite and GO resulting in graphene.

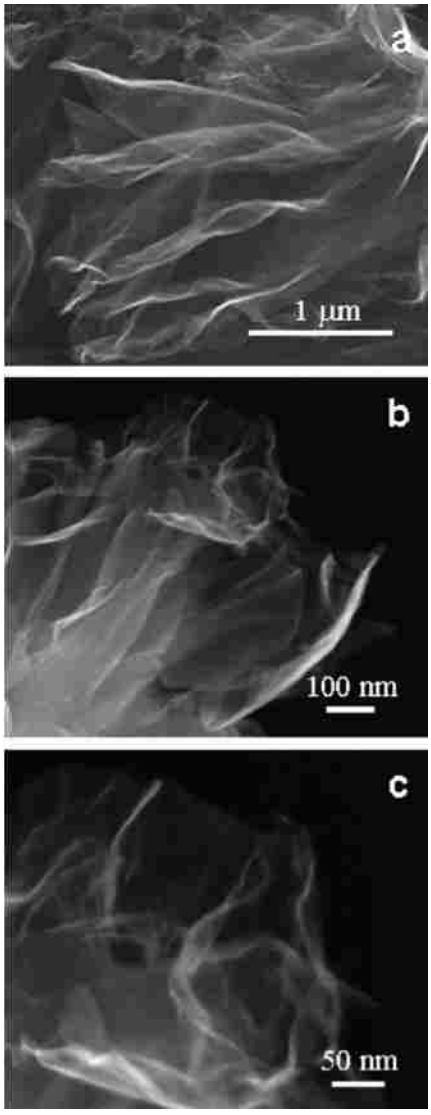

Figure 3.3: SEM micrographs of urea reduced sample (graphene sheets) as prepared. (a) and (b) loose open wave structures and extremely thin sheets are typical of the sample. (c) Inset of upper region of image (b).

TEM observation of a sample produced by the reaction of graphite oxide and urea at 600 °C, with no solvents involved in the sample preparation, is presented in Figure 3.4. The existence of extended thin layers, in some instances showing overlapping sheets, and individual sheets of graphene were characteristic of the sample. EELS analysis of the same sample (Figure 3.4d) showed peaks corresponding to a sp2 configuration, characteristic of a structure where bonds are all in same plane, forming a single 2D carbon arrangement (ca. 120° angle between bonds that naturally builds the hexagonal network present in graphene sheets). The inset in the figure corresponds to the EELS spectra of

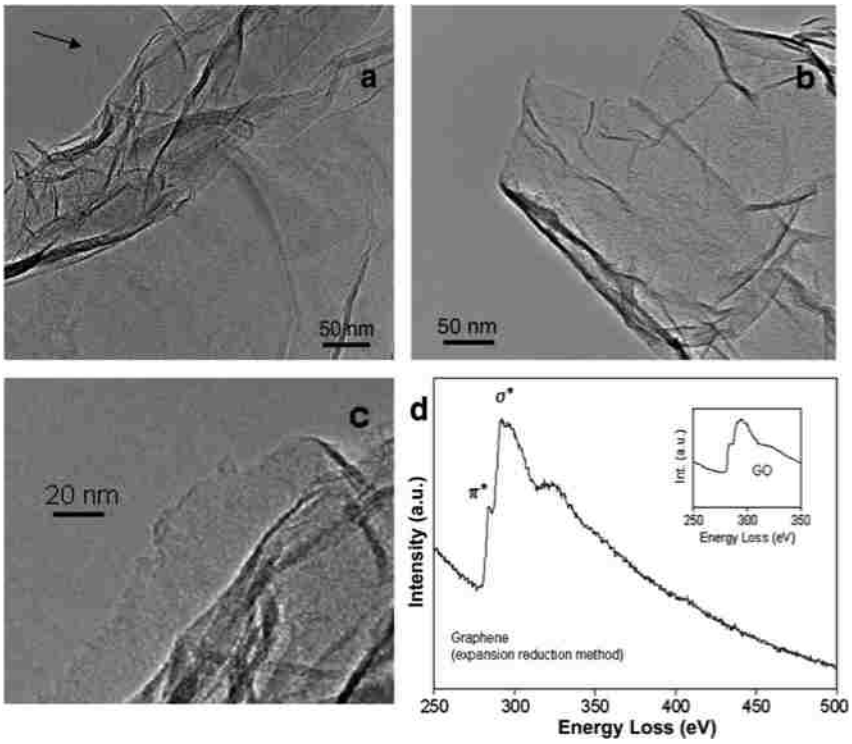

Figure 3.4: TEM images of the reduced graphite oxide (graphene sheets produced by the reaction of graphite oxide with urea at 600°C. (a) and (b) show the existence of thin extended films and (c) presents an inset of (a) in the region denoted by the arrow. (d) EELS spectra of the graphene sample generated by urea mediated expansion-reduction method. Inset: EELS spectra of graphite oxide.

graphite oxide, while the main spectra in the figure corresponds to the graphene product generated by the urea process. The main spectra showed well defined maximums for the carbon K ionization edge, close to 285 and 292 eV, which are known to correspond to the π* and σ* peaks of graphene-like structures [27, 51].

Samples produced at higher temperatures (ca. 800 °C) showed similar morphological characteristics when compared to the ones generated at 600 °C. Synthesis carried out for very short periods of time (5 minutes) presented extensive evidence of exfoliation and sample reduction. Nitrogen content in graphene samples produced from 1:1 graphite oxide:urea molar ratios were

found to be approximately 1.8%, while graphene from molar ratios 1:2 (urea 2·) contained 4.8% nitrogen. Oxygen content was found to be 36% for the original GO, 2.6% for samples treated with urea in a GO/urea 1:2 M ratio, and 0.6% for GO/urea 1:1 M ratio. This result points to molar ratios of GO/urea of 1:1 as precursors of graphene with less surface functional groups.

In order to elucidate the role of urea in expansion-reduction synthesis and differentiate between the processes presented herein from those that involve simple thermal exfoliation, GO samples without urea were heated in N_2 atmospheres in diverse conditions and variable heating rates. In all cases, the exfoliated samples without urea presented oxygen contents larger than 8%, even for heating treatments above 1000 °C.

During the reaction of graphite oxide and urea a white powder condensed in the exhaust lines of the reactor. Its XRD pattern had low intensity peaks, considerable background noise, and also displayed some reflections that coincided with urea, and a few peaks at approximately 20° and 30° (2θ) that could not be identified.

3.4.2 Expansion–Reduction Process Mediated by Urea

The use of urea to generate reducing gases is not new. The gas phase reduction reactions in selective catalytic reduction (SCR), long used to remove NO_x from stationary power plant exhaust, involve either: the use of NH_3 to reduce NO_x to N_2 and H_2O, or the use of urea to reduce NO_x to N_2, H_20, CO_2 [52-54]. A

more recent example is the use of urea as an expanding/reducing agent used to create metal and alloy nanoparticles from salts [55].

In the specific case described herein, we believe the urea decomposition promoted both the reduction and exfoliation of graphite oxide to produce graphene. First, a rapidly expanding gas was created by thermally decomposing the solid expansion–reduction agent. This gas had two functions in the process. The local 'shock' created by the rapid expansion of the gas separated the layers of the solid graphite oxide and exposed more of the material's surface. Second, the reducing species generated by thermally decomposing the expansion–reducing solid combined with oxygen and oxygen-containing groups on the carbon surface to form stable gaseous compounds and leave a reduced carbon product. The thermogravimetric/differential scanning calorimetric analysis of urea and graphite oxide mixtures under N_2 atmosphere showed a multi-step process. The steps can be correlated with similar features reported for 'neat' urea decomposition, plus a weight loss corresponding to the oxygen groups attached to graphite oxide. The breakup of the urea molecule is a complex reaction. It is known that the initial decomposition products exhibit high reactivity and can easily advance to secondary reactions [47, 56]. The thermal decomposition products of urea include biuret, cyanuric acid, ammeline, ammelide, $(HNCO)_x$, NH_3 and diverse polymeric substances, depending on reaction conditions. The thermal decomposition of urea in inert atmospheres happens at moderate temperatures (below 600 °C) although moisture and catalysts can alter the

process [57]. In any case, the decomposition steps of urea or similar compounds imply the generation of derivatives that can act as reducing agents.

The article published by Schaber et al. [56] was used as guidance to identify and correlate our process steps. Figure 3.5 presents TGA (upper) and DSC (bottom) graphs of the graphite oxide–urea mixtures subjected to the expansion–reduction process. In the DSC signal graph for urea decomposition, we can observe first an endothermic peak close to 150 °C, commonly associated with urea's melting point. This usually implies a vaporization process and decomposition into ammonium cyanate, which then immediately evolves into ammonia and cyanic acid (I). The process continues through the reaction of cyanic acid and remnant urea either to produce biuret (biuret decomposition: peak close to 250 °C) or to polymerize into cyanuric acid (II).

Higher temperatures can lead to the total decompostion of biuret, producing additional cyanic acid (major component round 300 °C) and ammonia, or cyanuric acid reactions with ammonia to form ammelide.

It is worth noting that cyanic acid reaction with water will produce CO_2 and NH_3. At temperatures close to 350 °C, ammelide and derivatives (ammeline) sublime and substantial amount of NH3 is lost while cyanuric acid decomposes significantly(III). Cyanuric acid decomposition is complete around 380 °C. Ammeline melts with decomposition at 435 °C.

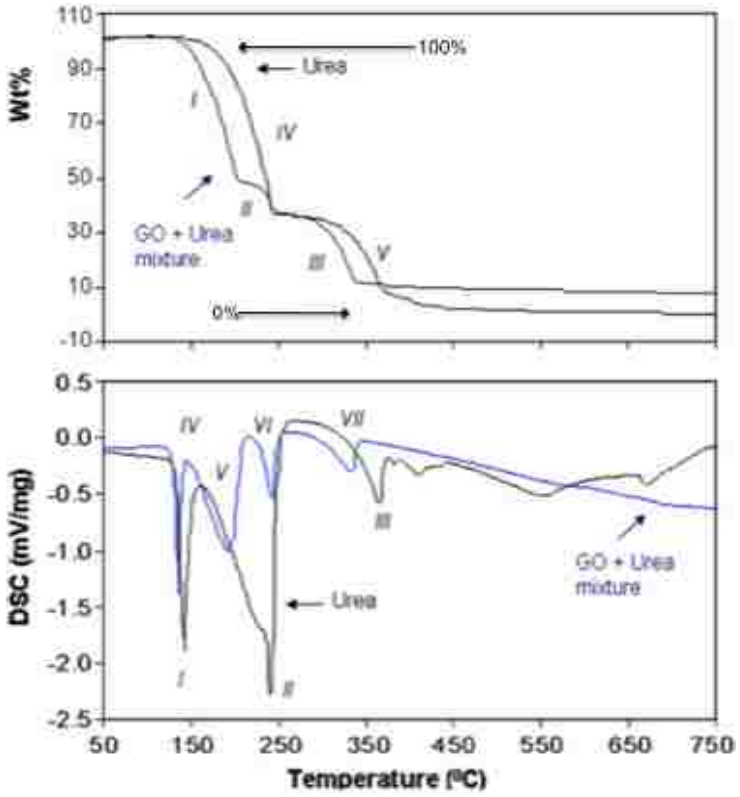

Figure 3.5: TGA/DSC analysis of a mixture of graphite oxide with urea treated under N_2 atmospheres. Upper graph: TGA signal. Lower graph: DSC signal.

The main difference between the study of the urea thermolysis presented in Figure 3.5 and the study of the thermal dissociation of the GO/urea mixtures is the clear separation of the peak close to 250 °C, forming two well defined peaks, one close to 200 °C (Point V) and one at 250 °C (VI). The third peak, located at 365 °C for urea, shifted to 335 °C (VII) for the GO/urea mixture. The urea thermolysis showed peaks at higher temperatures, usually associated with a complete decomposition of ammelide and ammeline, while the GO/urea graph presented the peak at 335 °C as the final transition. Our interpretation of these

results suggests the hydrolysis of HNCO when reacting with oxygen groups of graphite oxide at temperatures close to 200 °C, generating NH_3 and CO_2. Only very small amounts of biuret seemed to be present in the sample, giving rise to peak (VI). We considered its decomposition into ammelide and ammeline as negligible. Cyanuric acid formed in small amounts and decomposed earlier in the process (VII).

TGA analysis supports this interpretation. Weight losses for urea thermolysis seemed to occur in three stages: the first stage (IV) was related to urea decomposition to render biuret and volatile products; the second stage corresponded to the generation of cyanic acid and volatile materials (V); biuret formed in the third stage and decomposed into cyanuric acid and volatile substances (VI). The urea decomposed completely into volatile products with a total weight loss close to 600 °C. The weight loss associataed with the GO/urea reaction followed a similar path as urea, although the two stages for the process identified by DSC also are evidenced by TGA analysis; an initial weight loss occured below 200 °C, followed by a small weight loss during the formation of a stable product at 250 °C, which eventually reacts before 350 °C, providing a stable product whose final weight corresponds to reduced graphene. Graphite oxide loses all of its water molecules around 160 °C. We believe the water loss is associated with the hydrolysis of cyanic acid and the generation of NH_3 and CO_2 mentioned before. Oxygen groups in the reaction environment (from graphite oxide) could be connected with the oxidization of NH_3 to N_2 at

temperatures above 250 °C as well.

To our knowledge no other studies have been performed that have shown the reducing potential of urea when reacted with graphite oxide. Graphite oxide absorption of ammonia has been studied [58], although no thermal studies were done above 200 °C, and no attempt to reduce the sample by this means were undertaken. Urea's decomposition and emission of reducing gases temperature is much lower (well below 600 °C) than the final temperature used for thermal exfoliation of graphite oxide (1050 °C), which gives this method an advantage for mass production of graphene when compared to methods employing high temperatures in terms of oxygen species removal. In terms of exfoliation, thermal processes seem to be more effective, evidenced by the volumes of samples generated using both treatments. The use of urea in the process depicted herein is crucial: simple thermal exfoliation requires the heating rates to be large in order to promote gas evolution that generate enough pressure to overcome the van der Waals attraction between the layers and removal of the functional groups. The use of urea exacerbates the gas evolution process in a broader window of heating protocols, while the reducing species produced from its decomposition aid in the removal of oxygen groups. This yields graphene samples with lower oxygen contents. Concomitantly, higher nitrogen contents (between 2% and 5%) are observed in these samples. Moreover, the expansion-reduction process is based on technology that utilizes harmless reagents that are available in large quantities. Our work represents a proof of concept for the use of urea as an

expansion–reduction agent in the generation of finely divided carbon nanostructures with adequate characteristics for the applications that have been envisioned for graphene. In summary, the process presented in this article uses only moderate temperatures to reduce and expand graphite oxide into graphene and can be easily scaled up, in an extremely rapid and inexpensive fashion.

3.4.3 Attempts to Expand Urea-Mediated Process to Graphite

The product characteristics of graphite, and of graphite/urea samples were compared after undergoing the same thermal treatments. It was found that the expansion–reduction method does not lead to the exfoliation of pure graphite. Clearly, GO is required as a precursor to create graphene when using this process. SEM results showed that the thermally treated graphite sample (Figure 3.6a) presented the expected laminar structure, although more compact in form than the microstructure for graphite oxide prepared by Hummers method (Figure 3.6b). After reaction with urea at moderate temperatures, most of the graphite layers remained the same (Figure 3.6c), although a very small portion of the sample showed incipient exfoliation (Figure 3.6d). We believe that the urea decomposition products were unable to break the bonds between the unexposed graphene layers. The expansion–reduction process observed in graphite oxide might also be successful in other graphite structures that already contain surface functionalities, e.g. intercalation compounds.

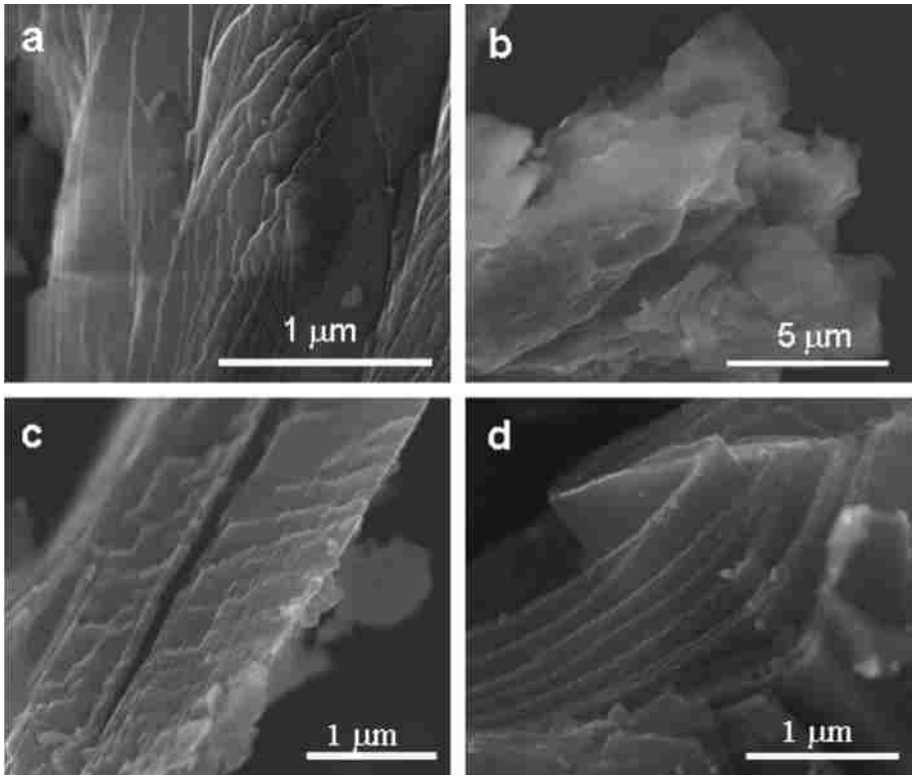

Figure 3.6: SEM images of attempts to apply urea mediated expansion-reduction method to graphite flakes. Only (d) shows slight exfoliation, thus this process only works with GO.

3.5 Summary of Expansion-Reduction Methods

We developed a novel method to generate graphene directly from a graphite oxide and urea mixture. This method involves the expansion and reduction of the layers of graphite oxide as urea decomposes. Advantages of this method include: an operating temperature much lower than required to simply exfoliate graphite oxide or graphite, a short reaction time, and a low concentration of oxygen surface groups.

While the reducing gases produced by the decomposition of urea remove the oxygen groups from the surfaces of the graphene, the gases also attach nitrogen to the graphene. These nitrogen surface groups seem to be comparable to doping the graphene with nitrogen. By “doping” the graphene with nitrogen, we seem to be able to improve the material’s capacitance. This phenomenon is discussed further in Chapter 5.

The expansion-reduction process is also a dry process, thus there is no need to use, and subsequently remove solvents or stabilizers as is required when using colloidal methods to generating graphene. All of the required materials are inexpensive, safe, and abundant.

Chapter 4
Procedure for the Evaluation of Electrical Properties and Contributing Variables

4.1 Characterization Methods

Once carbon products were generated using plasma and expansion-reduction synthesis methods, the samples (graphitic and amorphous carbon nanoparticles made from anthracene, carbon sheets/particles made from hexane, graphene form ethylene, and graphene made by expansion-reduction method with urea) were further characterized to determine how some of their features affected their performance as EDLC electrodes. The focus of this section of the manuscript is the methods used to determine the capacitive effects caused by microstructural variables such as: surface area, surface functionality, level of graphitization, and morphology.

4.1.1 Surface Area Analysis

Brunauer-Emmet-Tellet (BET) analysis was used to determine the surface area of each of the carbon samples: plasma generated graphitic and amorphous carbon nanoparticles made from anthracene, carbon sheets/particles made from hexane, graphene form ethylene, and graphene made by expansion-reduction method with urea. BET analysis is based on the mechanism of gas molecules adsorption on a solid surface. The concepts that are the basis for the BET theory are an extension of the Langmuir theory, and the theories that: gas molecules physically adsorb on a solid surface in layers infinitely, and that none of the

adsorption layers interact with each other. The validity of this theory and its legitimacy as a method to determine the surface area of a material is discussed by Brunauer et al. [59].

Surface area is an important factor in determining the activity and performance of finely divided materials. The surface area value provides a measure of how much of a solid material is exposed area. When the surface area of a substance increases, the rate of reactivity increases as well.

Physical gas adsorption techniques such as BET, can be used not only to determine surface area, but also to estimate pore volume and average pore size. In practice, the solid sample will be placed in a container of know volume. The gas in the container then is evacuated and a flow of pure nitrogen gas is introduced. The sample adsorbs the gas while the pressure in the container is monitored. Once a target pressure is reached, the gas flow is halted. The pressure continues to be monitored until it ceases to fluctuate and equilibrium is reached. The amount of gas introduced in the container, the volume of the system, and the final pressure are used to calculate the amount of gas adsorbed. The calculation of adsorbed gas is then used to determine surface area, pore volume, and pore diameter. In this study, N_2 adsorption/desorption on samples was measured using a Micrometrics ASAP 2020 or a Micrometrics Tristar 3000 sorptometer.

4.1.2 Surface Functionality

The surface groups located on the exposed area of carbon materials can have dramatic effects on the materials' properties and reactivity. For many applications such as semiconductors, fuel cells, adhesives, catalyst supports, structural fibers, and sensor devices, among others, the carbon material must be activated (i.e., exposed to specific atmospheres) in order to acquire the adequate surface chemistry for a specific use. The surface groups encountered on carbon materials can change how interactions at the interfaces between the carbon solid and other solid, gas or liquid materials take place. For example, highly hydrophobic surfaces can be turned hydrophilic, and vice versa, by changing the terminal groups at a material's surface. By engineering a material's surface, one can incorporate elements or functional groups that produce desired effects on the surface properties. In our case, due to time limitations, we only attempted to characterize the surface groups of the produced carbon samples rather than modify them. Several methods could be used to analyze a material's surface. These include x-ray photoelectron spectroscopy (XPS), electron energy loss spectroscopy (EELS), mass spectroscopy (MS), point-of-zero-charge measurements (PZC), and ion scattering spectroscopy (ISS), among others.

Since the carbon products of concern in this work were to be primarily exposed to a liquid interface (electrolyte) during their testing as EDLC electrodes, we limited our study of their surfaces to the use of MS and PZC measurements. Mass spectroscopy was used to analyze the percentage of oxygen and nitrogen

in the graphene sample generated by the expansion-reduction process involving urea and a thermally generated graphene sample that was used for comparison. PZC measurements were performed for all five (plasma and expansion-reduction) carbonaceous materials. The behavior of a solution-based interface, such as the interface in an EDLC test cell, will be affected by surface charges and their distribution. We considered that PZC measurements were a more appropriate way to characterize our carbon electrodes and determine whether their surfaces were positively or negatively charged.

For each carbonaceous sample, twelve 2mg specimens were weighed and placed into 1.5 dram glass vials. The top of the vials had been cut off to accommodate the Oakton Acorn series pH 6 meter's probe. One 0.04ml of ethanol was added to a vial using a plastic pipet. This step was taken immediately before the pH solution was added. Ethanol was necessary for the dispersion of the nanomaterials in the pH solution due to the samples' hydrophobicity. A glass pipet was primed with the pH solution needed, and 1.8 mL of the respective solution was added to the carbon sample. The sample then was immediately sonicated for 30 seconds using a Branson 2501 ultrasonic bath. After one minute, the pH of the sample was then measured and recorded. Next, the vial containing the carbon sample was placed on a Rotomix 48200 rotomixer for one hour. Meanwhile, the glass pipet was rinsed, using DI water, then ethanol. After that, the pipette was primed using the next pH solution to be mixed with carbon, then the pH meter was rinsed with DI water and primed with the

same pH solution that was used to prime the pipette. The process was repeated for all the samples. After each sample had mixed for an hour on the rotomixer, the pH was measured a second time. The meter was rinsed and primed after every measurement. For a diagram of the measurement process, see Figure 4.1.

In order to analyze the PZC data, points were plotted in a two-dimensional coordinate system, with the horizontal components being the initial pH measurements of a sample, and the vertical components of the points being the final measured pH. Once all the pH measurements were plotted, a curve is fit to the sample data. The second derivative of these curves allows for the calculation of the inflection points of each curve, which correspond to a point-of-zero-charge of a sample.

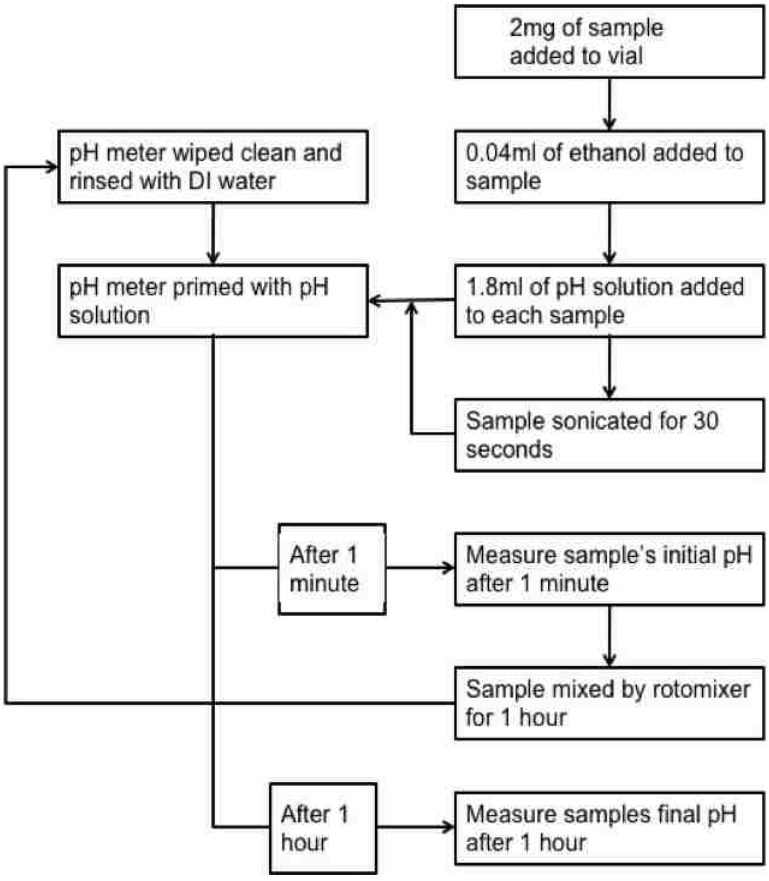

Figure 4.1: Flow chart illustrating point-of-zero-charge measurement process

4.1.3 Percentage of Graphitic Material

It is know that graphitic carbon is much more electrically conductive than carbon materials with an amorphous structure. Because of the differences in electrical properties between graphitic and amorphous carbons, our group thought it necessary to study the effects of graphitization on a material's capacitance to determine the importance of crystallinity when selecting an electrode material. These results are summarized in section 5.6.

There are several ways to measure the amount of crystalline material in a sample. Some methods are related to X-ray diffraction (XRD), others to electron diffraction (ED) of multiple points in a sample when observed using a Transmission Electron Microscope (TEM). Differential Scanning Calorimetry typically is used for polymeric materials, and Thermal Programmed Oxidation (TPO) for multiple types of crystalline/amorphous mixtures. For our study, TPO was selected as the most appropriate technique to study the level of graphitization for the range of diverse samples.

TPO analysis generally involves the controlled heating of a small amount of sample in a crucible as gases are passed through the furnace area, over the sample material. The sample-containing crucible is mounted to a highly sensitive balance that monitors the weight change of a sample during the course of the measurement process. The gases' flow rates also are highly controlled, as well as their concentrations in the instrument's atmosphere. The byproducts of the reaction process are carried out of the furnace by the flow of process gasses.

When carbon samples are treated in an oxidant environment at moderate temperatures, the oxidation mechanisms consist of a series of physical and chemical steps. Non-catalyzed oxidation typically follows the route: (1) transport of oxidant to the graphite surface; (2) adsorption of oxidant onto the graphite surface (physisorption); (3) formation of carbon-oxygen bonds (chemisorption); (4) breaking of the carbon-carbon bonds; (5) desorption of carbon monoxide, or other product; and finally (6) transport of reaction product from the carbon surface. Any of the above steps may be rate controlling (i.e., develop the major reactant concentration gradient).

For each material synthesized using the torch method, Temperature Programmed Oxidation (TPO) analysis was carried out in a Netzch STA 409, in which the samples' burn off processes were studied under 95%/5%, N_2/O_2 atmospheres (60 ml/min) with heating rates of 5 °C/min from room temperature to 900 °C.

It is known that graphitic material begins to burn at temperatures near or above 650 °C. By calculating the difference in weights at temperatures of 650°C and 830 °C, we were able to determine how much of each material was crystalline. It can be seen from inspection of the TPO data that each material has a different onset point, a temperature at which the material burns off completely. There are several reasons other than the material having a graphitic structure that may contribute to the onset temperatures of each material varying considerably. These factors include the particle size of each material and, in the

case of hexane, remnants of the precursor that may have wet the final product. It is for these reasons that we chose to quantify the level of graphitic material using the temperature of 650°C instead of using the individual onset temperature of each material, previously listed in section 2.3.

Although the results of the level of graphitic material (derived through the analysis of the TPO data) are only qualitative, the results are additionally reinforced by the examination of each sample through TEM. The levels of graphitic material reported are supported by visual inspection of the various TEM images in chapters 2 and 3. It should also be noted that powder x-ray diffraction (XRD) was also employed to analyze the crystal structure of each material. XRD analysis also supports the results reported levels of graphitic material, and an example of the graphitic nature of the plasma torch product synthesized using ethylene can be found in Figure 2.6.

4.1.4 Morphology

As mentioned in earlier sections, the carbon products morphology was studied by TEM and SEM analysis methods. The morphological studies of the materials are summarized in table 4.1. The particle size distributions of the amorphous nanoparticles and graphitic nanoparticles from anthracene are shown in Figure 4.2

Table 4.1: Tabulated morphological characteristics of all samples

Sample	Morphology
Amorphous NPs	Particles 10-20nm; Amorphous, spherical particles;no evidence of other morphologies
Graphitic NPs	Particles 5-25nm; uniform, spherical, graphitic particles, and a few graphitic platlets
NPs/Sheets from Hexane	Agglomerated, amorphous particles mixed with a small number of short thin graphitic sheets
Graphene from Ethylene	Very thin extended sheets of graphene (filter), and crumpled balls of graphene (torch)
Graphene from Urea	clustered, very large sheets of graphene; lengths on the order of 10's of microns

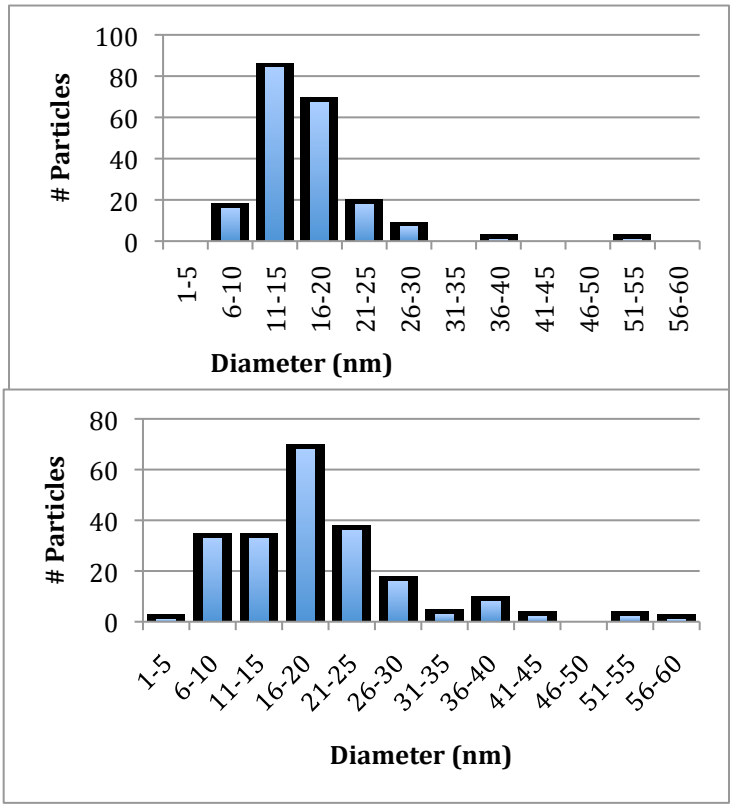

Figure 4.2: Particle size distributions of amorphous nanoparticles (top) and graphitic nanoparitcles (bottom) from anthracene

4.2 EDLC Assembly and Measurement of Electrical Properties

4.2.1 EDLC Assembly

As discussed previously, an EDLC test cell consisted of three main components: two electrodes composed of the carbonaceous material that we evaluated, an electrolyte that wets the electrodes, and a membrane that separates the electrodes but allows the movement of ions and charged particles between the carbonaceous electrodes.

We chose to use a Celgard 3501, 25μm microporous monolayer membrane (PP), surfactant-coated. In order to apply a current evenly across each electrode, the carbonaceous material being tested was formed into a paste and spread across a 0.025 mm thick piece of nickel foil (Alfa Aesar). However, in order to achieve a smooth surface on which to deposit the electrode paste, the Ni foil was attached (using super glue) to a (50.8mm x 50.8mm x 5.1mm) piece of glass, which had been cut using a RMX Products Glass Knife Maker. This Ni foil-glass assembly is known as a current collector. Once the foil was mounted to the glass, all excess foil was removed (to mirror the dimensions of the glass) except a small tab that was left extending out from the current collector. The foil tab acted as the contact point to connect the test cell to the measurement device.

The electrode paste was created by mixing 0.04mL of ethanol per 1mg of carbonaceous material. The solution of carbon material and ethanol then was sonicated for two minutes in a Branson 2510 ultrasonic bath. The ratio of carbon

material to ethanol, and the subsequent sonication produced a well-dispersed, ink-like solution.

A liquid polymer binder, (polytetrafluoroethylene 60 wt% dispersion in water [Aldrich]), further diluted with DI water, then was added to the solution of carbon material and ethanol. The binder was added in a ratio of approximately 8% binder, 92% carbon material. Binder is a necessary component of the electrode paste because it holds the electrode material together, which creates a more robust electrode once the paste has dried. The binder also contributes to the internal resistance of the EDLC test cell. As a result, a concerted effort was made to minimize the amount of binder used. Once the binder was added, the mixture was shaken for 30 seconds, sonicated for two minutes, and then shaken again for another 30 seconds. See Figure 4.3 for an illustration of the procedure used to synthesize the electrode paste.

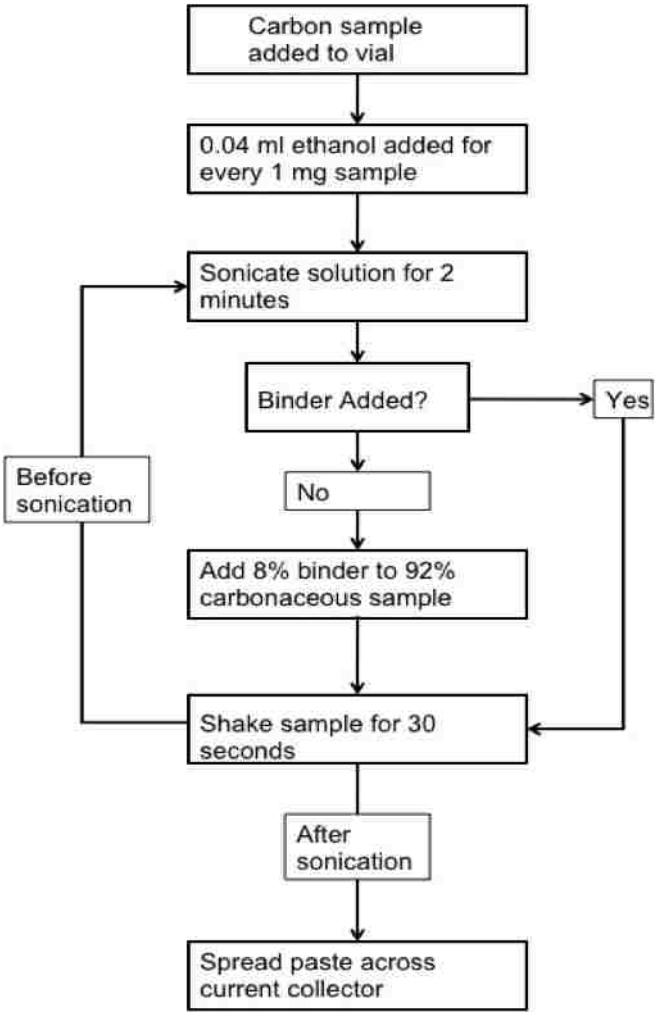

Figure 4.3: Flow chart for electrode paste synthesis

A portion of the electrode paste was then deposited on top of the current collector and spread evenly using the narrow edge of a glass slide. Two shims were placed on opposite sides of the current collectors. The shims were made from glass of the same thickness as the glass used in the current collectors. Three strips of stainless steel shim material (0.05mm thick) were stacked on top of each other and glued to the glass. Each glass/metal shim totaled 6.477mm in thickness. The glass slide that was used to spread the electrode paste traversed both of the shims; the extra height added by the metal shim material produced a gap of approximately 0.56mm between the slide and the current collector, insuring the paste was deposited evenly, with a uniform thickness. The deposition of the paste can be seen in the "before and after" photographs in Figure 4.4.

(a) (b)

Figure 4.4: Current collectors and glass shims (a) before electrode paste deposition and (b) after deposition.

To obtain a clean, flat work surface, the glass shims (glass and metal assembly) and current collectors were attached to a ceramic tile. The glass shims were taped down, but the current collectors were simply held in place with moldable clay.

It was found that elevated levels of humidity resulted in the electrode paste cracking if left to dry in the open atmosphere. To combat this phenomenon and to minimize foreign particulates depositing on the *electrode* (current collector with electrode paste), the electrodes were removed from the tile and shim assembly and left to dry in a large hermetic box filled with desiccant. Once the paste had dried, the electrodes were assembled into an EDLC test cell. It should be mentioned that, before glass was used as the electrode substrate, stainless steel current collectors were used instead. The stainless steel current collectors were part of an intricate test cell that could be sealed and bolted together (Figure 4.5).

(a) (b)

Figure 4.5: Initial attempts at an EDLC test cell. Open, with current collectors exposed (a) and bolted together, fully assembled (b)

However, when these test cells were assembled, it was very difficult to prevent the electrodes from slipping and shorting out. The electrode paste was deposited directly onto the stainless steel current collectors in an effort to eliminate the slipping effect. Ultimately, the finished surface of the stainless steel was too coarse to accommodate a thin layer of electrode paste without the paste cracking once it dried. As a result, we developed the EDLC test cells motioned previously to test all of our samples.

The electrolyte used in an EDLC test cell was a 1M solution of potassium hydroxide (VWR). 0.085mL of electrolyte was used for each test cell assembly. Instead of wetting the electrodes directly, a 30.5mm x 30.5 square piece of membrane was cut and an inner area (25.4mm x 25.4mm) of the membrane was masked. Next, the exposed edges of the membrane were lightly coated with petroleum jelly and the mask was removed. The inner area of membrane not coated with petroleum jelly was the area wetted with the electrolyte. By masking the outer edges of the membrane, we ensured that the electrodes would not short and that the wetted area was confined to a 25.4mm x 25.4mm area.

The wetted membrane was aligned and placed on top of one of the carbonaceous electrodes. The second carbonaceous electrode was aligned and placed on top of the membrane, sandwiching the membrane and electrolyte between the two carbonaceous electrodes. A balsa wood scaffolding was used to align the electrode-membrane-electrode assembly and prevent the components from shifting. The scaffolding was formed from two 43.2mm x

12.7mm pieces of balsa wood glue perpendicular to each other in a large Petri dish. Each rectangular piece of balsa wood was notched with a 33.1mm x 5.1mm hole. The vacant space eliminated any interference between the edges of the membrane or foil tab with the balsa wood support structure. The assembly of an EDLC test cell is illustrated in Figure 4.6.

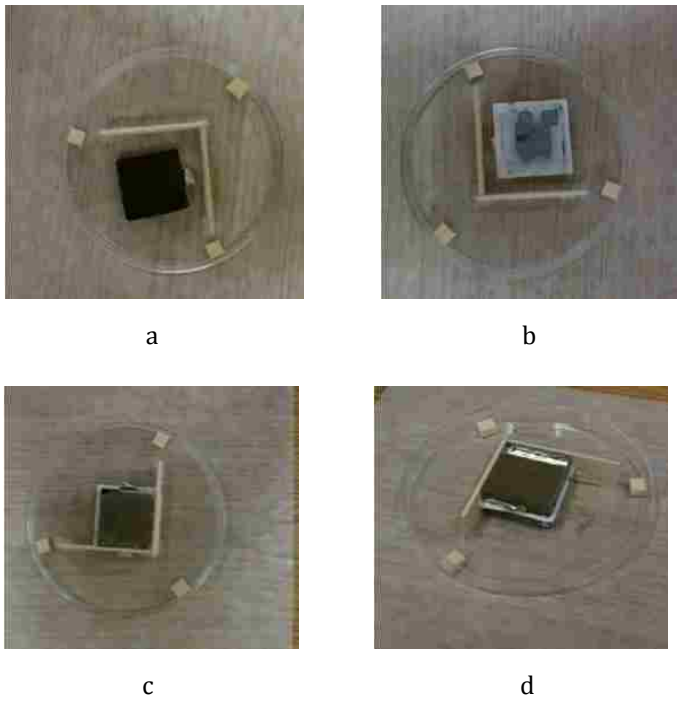

Figure 4.6: Assembly steps of an EDLC test cell: (a) the first electrode in placed face up in the scaffolding (b) the wetted membrane is aligned and placed on top of the electrode (c) the membrane is sandwiched between the two electrodes (d) the assembled EDLC test cell is supported by the scaffolding.

4.2.2 Electrical Measurement Methods

To measure the capacitive properties of each electrode material, we used a National Instruments ELVIS II+ 100MS/s Oscilloscope equipped with a National Insturments ELVS II Series Prototype Board. The ELVIS system applied a small voltage across the test cell, eventually providing a reading of maximum capacitance for each test cell. Each cell tested took only a few seconds to attain a maximum capacitance. The ELVIS system also was able to provide a measurement of the total resistance of each test cell. Unlike the measured capacitance, the value of resistance for an EDLC test cell took several minutes to attain a stable value.

In order to determine whether the Ni substrate contributed to the capacitance of an EDLC test cell, a cell without any carbonaceous electrode material was assembled. All of the other elements of the test cell remained the same. Without the carbonaceous material, the EDLC test cell was found to have only a nominal level of capacitance and resistance. Thus, the Ni foil made no significant contribution to either the capacitance or the resistance.

Chapter 5
Results and Discussions

5.1 Electrode Selection: Carbon

Diverse energy storage devices have traditionally included carbon, either as supports, substrates or conductive additives. The allotropes of carbon include both crystalline (graphite and nanotubes) and the amorphous (foams and aerogels) forms. The desired characteristics that a material has to present in order to be used as an electrode in an EDLC include a combination of chemical and physical properties: high conductivity, high surface area, controlled pore structure, temperature and corrosion resistance, general stability and, preferably, low cost. Owing to the fact that carbon possesses all of these properties and can be prepared in a wide range of structures, degrees of graphitization, dimensionality (3D, 2D) and is environmentally friendly, carbon constitutes the perfect candidate and is the reason carbonaceous products were selected for this work. Studies in the field of supercapacitors have been focused primarily on generating carbon electrode materials with high surface areas, with special emphasis on pore size distribution and low resistivity in the matrix.

In this work, we expanded the range of characteristics being studied. We examined the dependence of the capacitance values (measured in a double layer configuration) on the surface area, pore volume and diameter, level of graphitization, surface functionality and microstructural features (shape and size of particulates), as well as the resistivity of the electrode material.

Plasma torch based materials are known to have low amounts of surface / functional groups as prepared. These attributes gave us the opportunity to study the raw materials and then decide whether surface functionalities should be added in order to optimize cell performance in future studies. Activation processes also could be performed in order to increase surface areas. The basic microstructural characteristics of these carbon products were described in Chapter 2.

Graphene prepared using a reduction-expansion method (urea based) also was chosen as a material to study, because graphene production was rapid, rendered high yields, and the precursors were inexpensive. Once we understood the mechanism that dominated the graphene formation process when using urea, and the surface groups of the material were quantified, the graphene sample presented a good reference point for comparative studies with plasma fabricated samples. The basics of the expansion-reduction method are addressed in Chapter 3.

5.2 Electrolyte Selection

Water based electrolytes commonly used in supercapacitors can be acid (i.e. HCl or H2SO4) or basic (i.e. KOH). Their advantages when compared to organic electrolytes are the result of their high ionic conductivities and low costs. The main disadvantage of using aqueous electrolytes is that they present a very narrow window of voltage ranges, which is inherent to the low decomposition

voltage of water (close to 1.23 V). Published specific (F/g) capacitance of carbon electrodes used in aqueous electrolytes is much higher than the capacitance of the same electrodes using non-aqueous solutions that present higher dielectric constants[60]. While non-aqueous electrolytes have wider windows of operating conditions, their electrical resistivity is at least an order of magnitude higher than aqueous electrolytes, producing higher internal resistance capacitors. For reasons such as these, our studies were performed using KOH solutions as the electrolyte.

5.3 Binder and Porous Membrane

Because the carbonaceous materials to be used in supercapacitor devices are fabricated in a powder-like form, it becomes necessary to use an additive to integrate the sample particulates into a cohesive form, even when deposited as thin film. Such an additive is commonly referred as a binding agent and consists of a non-conductive substance that polymerizes and gives the sample structural integrity. Common binding agents include Teflon based polymers or PTFE (polytetraflouroethylene) chains. Given the polymeric nature of the binding agent, the edition of the binding agent decreases the electrical conductivity of the electrodes, which in turns adds to the preexisting interparticle and internal resistances. To avoid the formation of physically and electrically insulated carbon particles, only small amounts of binding additive should be employed (no

more than 10% in wt). The test cells studied in this work had 8% PTFE by weight incorporated in the electrodes.

Membrane separators used in electrical double layer capacitors must provide electrical insulation between the two electrodes layers while being ion permeable to allow charged species in the electrolyte to flow freely. From the membranes available commercially, (Celgard (polypropylene (PP), polyethylene (PE), or trilayer PP/PE/PP electrolytic membranes)) the Celgard membrane was chosen because it maintains its physical integrity as well as its chemical and thermal stability in the window of operating conditions in which our materials were tested.

5.4 Capacitance Values

The amount of research regarding carbon electrode materials to be used in energy storage applications has grown markedly in the last decade. The same types of carbonaceous samples may be built in diverse configurations and added to different systems as essential elements in fuel cells, batteries and supercapacitors. The level of complexity of the systems employed has also multiplied due to a large number of variables: possible electrolytes, separators, configurations, working conditions and inherent characteristics of the materials used.

To this level of complexity we should also add the differences in the way capacitance values are reported. Values usually are given either in farads/gram

or farads/cc, depending on the author's preference for reporting data in gravimetric or volumetric units. The greatest challenge encountered during this investigation has been the development of protocols to measure the electrical properties of the samples, analyzing the data and explaining how the diverse variables studied in this thesis affected capacitance measurements. The main concern has been the lack of a standardized method to compare the performance of materials so the data can be used as a reference for a materials performance.

Since capacitance values are the basis of our comparisons and the measure by which the carbonaceous material characteristics and their effects are evaluated in this study, it is appropriate to review how capacitance values are reported: Devices based on double layer capacitance and high surface area substrates, so called supercapacitors, are named for the large capacitance values (compared to traditional and electrolytic capacitors) they exhibit. We will begin our data analysis by following the most conventional way to report capacitance data; we will refer to values of double layer capacitance or accessible capacitance in μF/g. The gravimetric measurements of capacitance we report refer only to the weight of the active material.

For example, a large surface area, porous electrode carbon material has $900 m^2/g$ and exhibits 14 μF (real cm^2) when in an electrolyte solution in a cell configuration. The accessible capacitance will then be: 900 (m^2/g) x 10,000(cm^2/m^2) x 14 (μF/g) = 126 F/g.

Upon further examination, and by plotting the amount of material (expressed as 1/wt (g^{-1})) against capacitance (μF/g), we found a clear correlation, i.e. smaller amounts of material will have higher values of capacitance, showing that the measured capacitance is a function of the amount of electrode material being used. See Figure 5.1 (top). An alternative way to analyze the measured data is to plot capacitance (μF/g) versus amount of material (g). See Figure 5.1 (bottom). This method yields similar results.

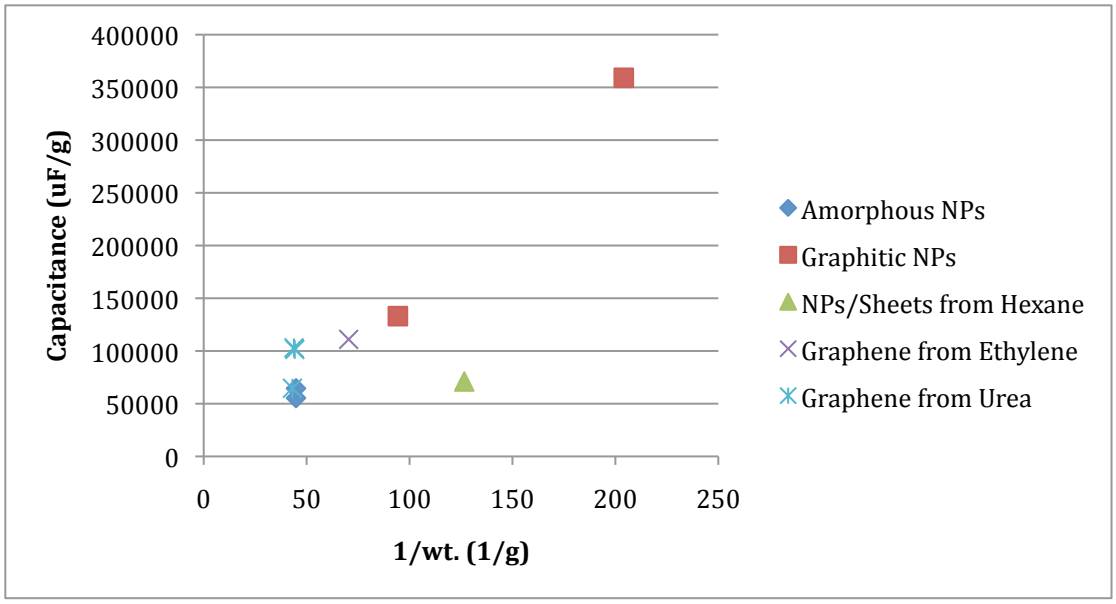

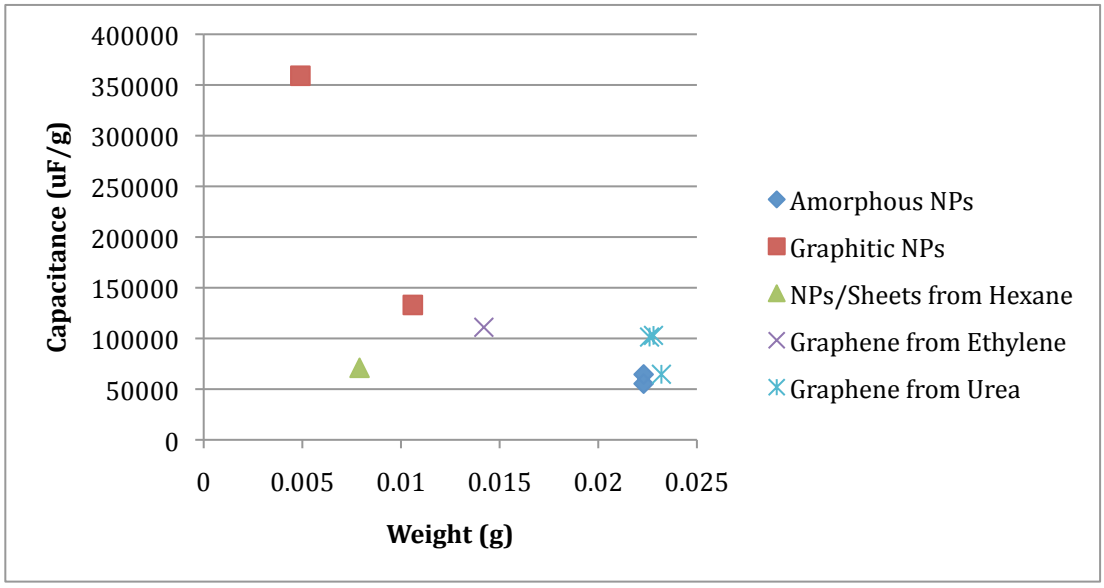

Figure 5.1: Material capacitance (μF/g) vs. 1/wt. (top) and capacitance (μF/g) vs. weight (bottom).

It is worth noting that the green triangles, corresponding to carbon samples prepared from hexane, seemed to be an outlier in some of the graphs. This effect is a result of very small amounts of liquid hexane wetting the end

product. This phenomenon was revealed by thermogravimetric analysis and is discussed in section 2.3.

Sections 5.5 to 5.8 present data relating surface area, pore characteristics, level of graphitization, point-of-zero-charge and microstructural features to capacitance given in μF/g. This preliminary data represents an initial effort to report electrical properties and performance of the materials when assembled in an EDLC. More detailed analysis is being conducted, through a collaboration with AFRL, in order to obtain cycling data.

5.5 Surface Areas and Pore Characteristics

Surface areas and pore-size distributions have been considered the two characteristics of an electrode material that most significantly affect capacitance values. We confirmed that surface area strongly influences the capacitances of the samples, and our data shows a good correlation between these values (higher surface areas produce higher capacitance). However, we also observed that targeting high surface area specimens alone is not enough to increase/optimize the capacitance values of a material. From the samples analyzed, we observed that some samples with relatively low surface areas exhibited capacitance values superior or equivalent to samples with 30% more surface area. See Figure 5.2. In particular, the graphene prepared by the expansion-reduction approach presented higher capacitance values than samples such as the amorphous nanoparticles that were prepared from

anthracene or the mixture of particles and sheets that were fabricated from hexane.

All the samples analyzed in this work, as well as most carbon materials used for electrodes, are derived from hydrocarbons that are heat treated under inert or reducing atmospheres. The final characteristics of such products depend on many factors, including precursor, aggregation state during carbonization, and conditions of the process. In the case of the plasma torch process, the precursors underwent a rapid thermal decomposition that eliminated all of the volatile materials and heteroatoms. In contrast, the expansion-reduction method began with graphite oxide and utilized urea to expand and reduce the sheets that contained the oxygen groups. This fabrication method eliminated most of the oxygen present in the original structure of graphite oxide. However it also introduced nitrogen species in the newly formed graphene. We believe the new effect, which is a result of the nitrogen groups present on the graphene, has a stronger effect on the graphene's electrical properties than the effects that are attributed to surface area.

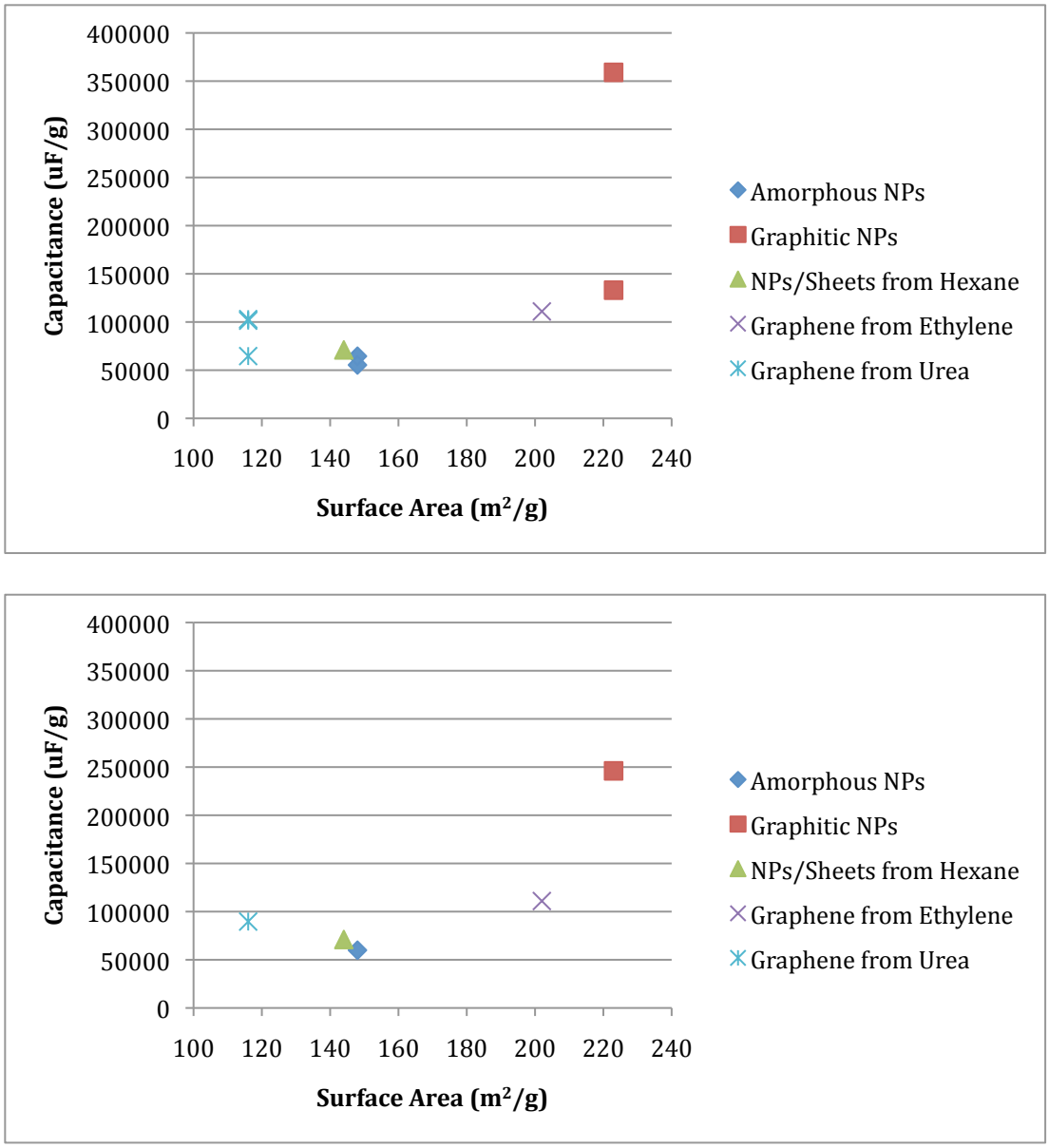

Figure 5.2: Surface area vs. capacitance for all samples measured (top) and the average capacitance vs. surface area for each sample (bottom)

Because the samples produced by plasma and expansion-reduction approaches generated carbon nanoparticles, graphene sheets and mixtures of both, analyzing pore volume and diameter may not have revealed the same

network characteristics as when the same techniques are used to analyze particulate porous structures. BET analysis also provides pore analysis, so we have presented the collected data. The literature in the field recognizes that only the electrolyte wetted surface area has a contribution in the capacitance, and surface area values are not enough to accurately describe the accessible surfaces that can be accessed by an electrolyte. The typical way to describe this phenomenon is to talk about “open” pores and the need to “activate” a material in order to open or generate more area that can be easily accessed by the electrolyte.

It is assumed that the surface area accessed by nitrogen gas during BET measurements is similar to surface area accessed by an electrolyte during capacitance. To the contrary, there are considerable differences between a nitrogen molecule that is expected to reach all open pores and an electrolyte, which has its own viscosity, dielectric constant, and other characteristics. The interactions between the electrolyte and the carbon interfaces (for example those derived from hydrophobicity of carbon surfaces) will have an influence on how the electrolyte penetrates the pores or open spaces of the solids. The values we obtained suggest that a sample’s capacitance is higher for larger pore volumes, except in the case of the graphitic nanoparticles, in which case the degree of graphitization might have a bigger influence on the capacitance than other factors. Instead of a linear relationship, the values of capacitance versus pore

volume for the amorphous particles, graphene from ethylene and particles/sheets from hexane, seem to follow a logarithmic behavior. See Figure 5.3 below.

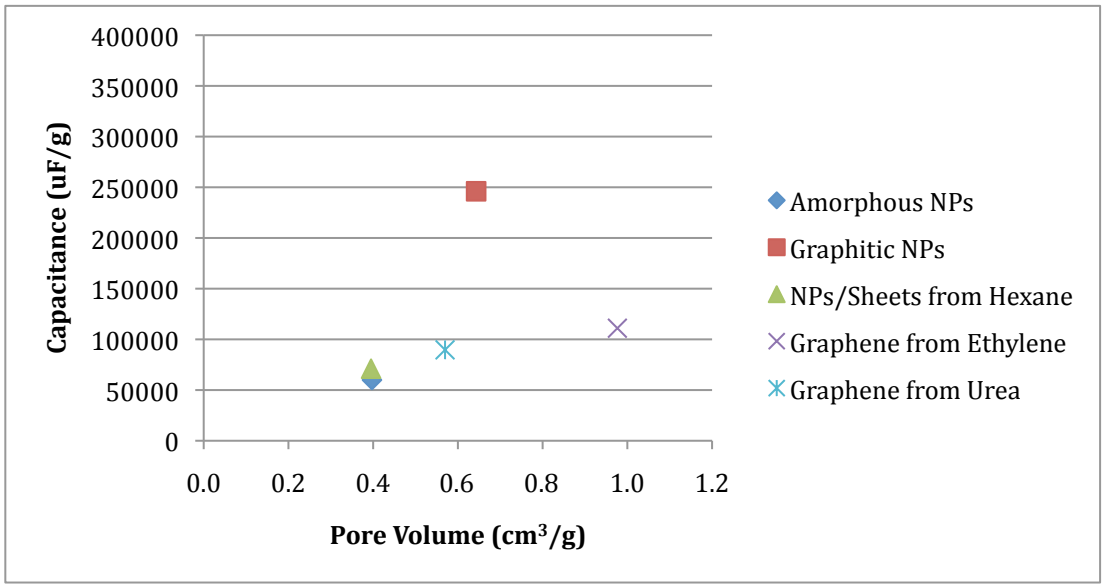

Figure 5.3: The averaged capacitances of each type of material plotted against the material's measured pore volume

When examining the pore diameters of each material, the relationship to capacitance is similar: the higher values of pore diameter consistently correspond with higher capacitance. The exception is the graphitic nanoparticles, which have the highest capacitance values. Figure 5.4 illustrates the relationship between capacitance and average pore diameter of a material.

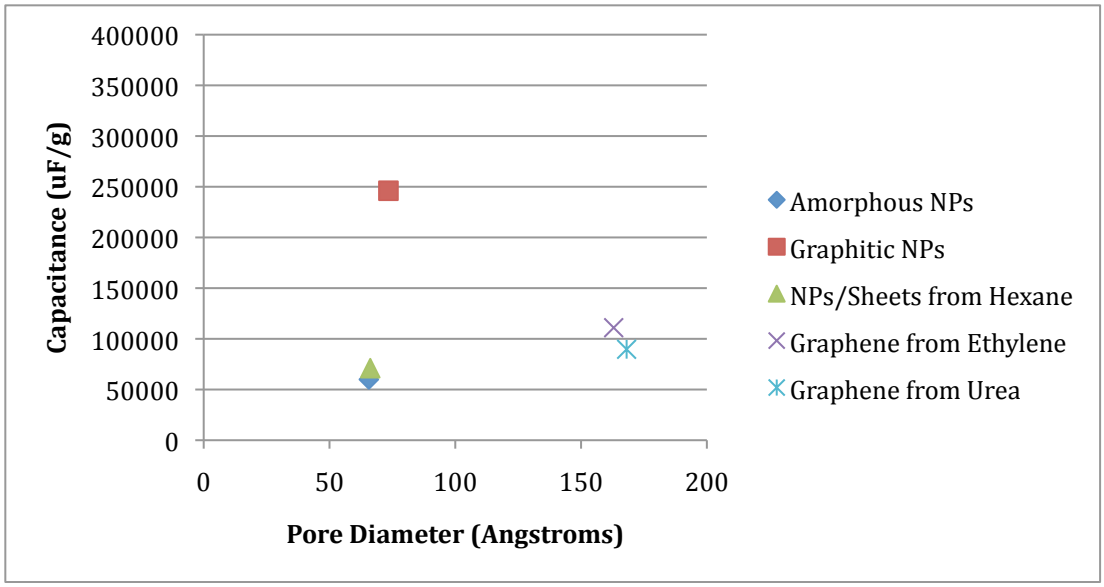

Figure 5.4: The average capacitance for each material plotted against the measured average pore diameter of each material

Using either thermal or chemical activation processes to increase additional porosity in the samples could be considered for the next generation of samples and future work.

5.6 Level of Graphitization and Internal Resistance

When the term "level of graphitization" is used, it is referring to the amount of material with long-range crystalline order, similar to the order that is found in graphite. In this study, graphitization occurred in several different forms such as graphene, graphitic particles and graphitic platelets.

The carbon materials produced were divided into two groups: the materials prepared by plasma torch method, and the material resulting from expansion-reduction synthesis. The primary reason for this division was the

nature of the process that generates each carbon product. The plasma made materials began as hydrocarbons that were pyrolyzed in an inert atmosphere and then condensed as carbon byproducts once all volatile materials evaporated. When condensation occurs (in the after glow region of torch), localized graphitic sites begin to grow and, depending on the conditions of the experiment, these sites may remain as small independent units (as is the case with nanoparticles) or align as sheets (such as graphene).

The nature of each precursor (solid, liquid or gas) also had a strong influence on the final form of the carbon product. Solid anthracene seemed to reach its decomposition temperature and lose volatile material to produce independent units that agglomerated, in the end forming spherical nanoparticles. The degree of graphitization of samples with short residence times in the hot zone, or discharge zone, of the plasma, was very small. This was a result of a insufficient time for the material to organize its structure and yielded amorphous nanoparticles. This mechanism suggests that during the carbonization process, once a material forms a solid, the limited mobility of crystallites results in a rigid, amorphous structure.

Only the effect of pressure and decreased aerosol flow rates in the system forced the materials to have longer residence times and reach temperatures that allowed graphitization to occur. These conditions resulted in graphitic nanoparticles from anthracene. The size and the orientation of crystallites are the key to the electrical conductivity of samples. As seen in most graphs presented

in chapter 5, graphitic nanoparticles seem to have the highest capacitance values.

Over pressure and reduced aerosol flow rates in the plasma system produced samples in which we found platelets, although these structures did not dominate the sample morphology, in spite of the fact that anthracene is a solid precursor. We concluded that the existence of the platelets is a result of the plasma's high temperatures that can vaporize the solid, during which time the sample undergoes an intermediate process (similar to the one observed in liquid and gases) that allows the material to assemble itself from a molecular precursor, rather than from a solid precursor. Higher system pressure conditions (10-15 torr above atmospheric pressure) are also responsible for lower yields.

Liquid and gas precursors (hexane and ethylene respectively) have shown a tendency to generate greater amounts of extended films (ca. graphene type structures) consistent with a carbonization process in which molecules pass through a fluid stage (mesophase) and align with each other to form a more extensive graphitic structure. Under sufficient conditions, molecules undergoing this mesophase will form sheets of graphene.

The materials generated by plasma torch processes observed the same general guidelines that have been reported previously [33, 61-63].

The expansion-reduction samples present a very different case. These specimens were made from graphite oxide, which is already a layered and crystalline material. These materials underwent an exfoliation and reduction

process instead of a vaporization and condensation process. The basic features of these samples (in terms of crystalline arrangement) were those of individual sheets, that is, a two dimensional lattice. The only difference observed was in the separation between sheets in the c direction.

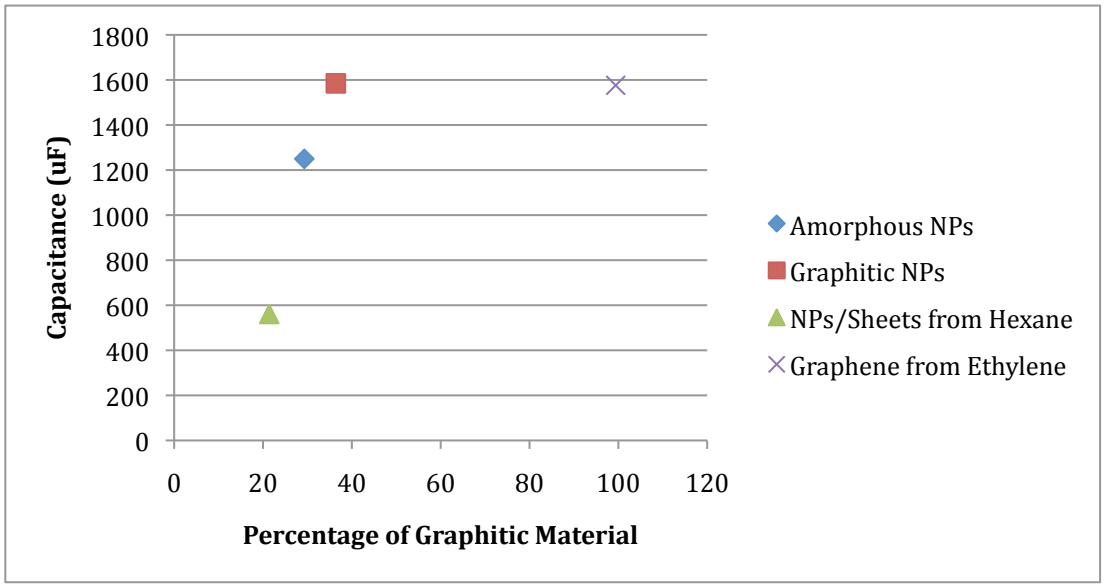

Figure 5.5: The capacitance of each sample plotted against the percentage of graphitic

Table 5.1: Remaining sample weights corresponding to the onset temperature, 650 °C, and 850 °C

	Onset Temp	Wt% @ Onset	Wt% @ 650 C	Wt% @ 830 C	uF
NP/Sheets from Hexane	518.7	57.1	27.6	6.3	561
Amorphous NPs	581.4	70.4	38.3	9.0	1250
Graphitic NPs	591.8	81.4	56.6	20.2	1585
Graphene from Ethylene	704.9	93.7	105.6	6.2	1576

The resistivity of materials that are used in electrode applications is crucial. The resistivity value is not only an intrinsic characteristic of the carbon material (intra particle), but also is a result of the microstructural characteristics of the material, such as the inter particle resistance.

The conductivity of carbon samples is dictated by the thermal history of the sample. When subjected to higher temperatures, the material develops more sp2 states. These states increase the conductivity associated with electrons in π bonds that are delocalized and become charge carriers [64].

Electrical conductivity also depends on the contact between each particle. Long inter particle distances will present a higher internal resistance, as observed in graphene produced by ethylene. In the later case, graphene sheets crumpled and formed spherical aggregates of hundreds of nanometers in the coupler region of the torch. Graphitic nanoparticles with average particle size distributions in the order of 15-17 nm appeared to have a more compact arrangement in the electrodes, which resulted in an interconnected, conducting network. We concluded this arrangement is responsible for the higher capacitance values observed in all capacitance graphs presented in this chapter.

Table 5.2: Resistance trend of carbon samples; Graphitic NPs show the least resistance and Amorphous NPs the highest

	kΩ
Graphitic NPs	13.007
NPs/Sheets from Hexane	14.211
Graphene from Urea	19.396
Graphene from Ethylene	24.668
Amorphous NPs	29.615

The presence or absence of surface functionalities in a particular carbon electrode can be associated with the conductivity of samples. Recent reports, from Rao et al [65] present evidence on how doping affects the electronic structure of graphene materials. In such, boron and nitrogen dopants were introduced into graphene structures to exhibit p- and n- type semiconducting electronic properties. Pure graphene is a zero band gap semiconductor, with its density of states at the Dirac point equal to zero [16], which limits its applications in electronic devices. Although there is a noteworthy difference between nitrogen doped graphene and graphene containing nitrogen surface groups, we can assume that the expansion-reduction method of synthesis produced samples with significant amounts of nitrogen (2 to 5%) and that these might be responsible for higher capacitance values and lower resistances than expected from the sample's surface areas and morphological features.

5.7 Surface Groups Given by PZC

Surface groups can drastically affect a material's wettability, electrical resistance, point-of-zero-charge and capacitance. Although there are several ways to classify carbon surfaces (i.e. basal and edge sites, concentration of heteroatoms (oxygen, nitrogen and sulfur typically)) the surface groups are classified as acidic, neutral and basic. Acidic functionalities are usually less stable and are commonly related to the reaction between carbon and oxygen at moderate temperatures (200-700 °C) [64]. Basic and neutral functionalities tend

to be more stable and form at the surface of carbon materials. Basic and neutral functionalities usually are a result of reactions with oxygen at low temperatures. Because the plasma synthesis was carried out in an inert atmosphere, and the temperatures that were reached where on the order of thousands of degrees (°C), we expected to obtain neutral and basic surface groups. Although the expansion-reduction approach removed the original oxygen functionalities present in the graphite oxide, we also could have expected, basic and neutral surface groups.

Point-of-zero-charge measurements revealed that all the samples exhibited pH values close to neutral: between 6.2 for the hexane particle mixtures and 7.5 for the graphitic nanoparticles from anthracene.

Table 5.3: The point-of-zero-charge trend for the carbonaceous samples; sample material from hexane shows the most acidic pH while the graphitic NPs show the most basic pH

	pH
NPs/Sheets from Hexane	6.19
Graphene from Ethylene	6.34
Graphene from Urea	6.75
Amorphous NPs	7.00
Graphitic NPs	7.51

Since all PZC values for carbon electrode materials prepared by plasma and expansion-reduction are very close to neutral pH, we can expect higher stabilities when the materials are incorporated into an EDLC test cell than materials of highly acidic or highly basic natures. Electrodes assembled from materials that are highly acidic or highly basic usually result in high rates of self-discharge and lower leakage currents[66].

Surface functionalities also help to explain why the samples of graphene from urea have higher capacitances than would be expected if one considered capacitance only as a function of surface area and porous qualities. Wang et. al [67] found that graphene could be functionalized with nitrogen by high-power electrical joule heating in ammonia gas to produce n-type electronic doped graphene. Wang et. al also found that it was necessary to have oxygen present during the reaction or to pre-oxidize the graphene before it was functionalized and that the degree of nitrogen doping scaled with the degree of oxidation or the concentration of defects in the graphene lattice.

One of the reducing gases urea produces as it decomposes is ammonia, and the graphitic material we used to produce graphene was already pre-oxidized (graphite oxide). Thus, we can assume that the resultant graphene produced from our expansion-reduction method also exhibits n-type electrical material properties. Moreover, our expansion-reduction method seems to eliminate the need for pre-oxidation steps and ammonia atmospheres. It is also possible that the removal of the oxygen from the graphite oxide surfaces produces defects in the graphene lattice, allowing for more doping.

5.8 Microstructural Features

The microstructures of all the materials studied are analyzed in detail in Chapters 2 and 3, and section 4.1.4 also briefly summarizes the morphology of each material. Figure 5.6 below illustrates the typical microstructure of each material and the resulting capacitance each type of microstructure produces.

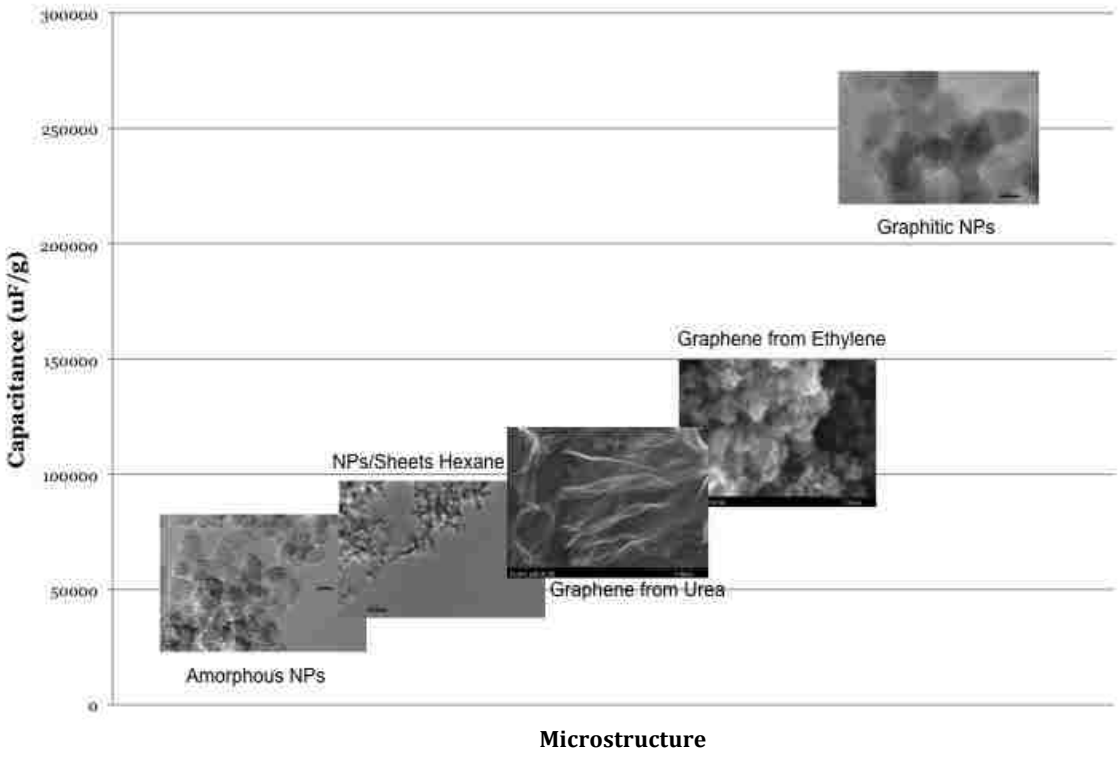

Figure 5.6: The resulting capacitances that result from each of the five different microstructures. *Note: Original Sample images can be found in chapters 2 and 3

5.9 Capacitance Conventions

Section 5.4 presented reasons to express capacitance as units of μF/g, which has become a common way to express the performance of EDLC devices and, indirectly, electrode behavior. A thorough inspection of the data illustrated in Figures 5.1 and 5.2 (in particular, data for the same type of material [same batch]), revealed that there was enough variability between samples of the same nature (i.e., graphitic carbon particles generated from anthracene) to question whether a combination of effects or additional variables exists that is not accounted for when expressing capacitance results in terms of μF/g.

Using basic theories of capacitive materials, we assumed that a supercapacitor consists of two electrodes, submerged in an electrolyte, with a separator in between each electrode/electrolyte interface. The complete EDLC cell is considered to be two capacitors in series, with a capacitance given by:

$$\frac{1}{C_{cell}} = \frac{1}{C_1} + \frac{1}{C_2}$$

where C_1 and C_2 represent the capacitance of each electrode. The double layer capacitance at each electrode interface is given by:

$$C_{dl} = \frac{\varepsilon A}{4\pi t}$$

where ε is the dielectric constant of the electrical double layer region, A is the surface area of the electrode and t is the thickness of the electrical double layer.

With such relationships in mind, we would expect that the capacitance values would be greatly affected by the thickness of the electrode layers. The thickness of an electrode could be related to a volumetric amount of material. Because an electrode's volume will change depending on the material's particulate arrangement or empty space, we were able to provide a different type of correlation by reporting capacitance vs. volume. In other words, a material's density (mass/volume) will differ between each sample depending on microstructure, thus normalizing by volume yields a more comprehensive value of capacitance.

In light of all this information and knowledge of the factors that can complicate a comparison of samples, we believe that, in the future comparing electrode performance using capacitance measurements will be more accurate when using its absolute value (farads) and calculating the material's dielectric constant. If two dielectric constants are not equal, we can assume that the electrode materials are different and that the differences between the materials manifest themselves as microstructural changes, surface functionalities, etc. In other words, we advocate for a change in the paradigm that all carbon materials have the same dielectric constant so we can precisely differentiate between carbon in it is diverse states: graphene versus thicker graphite layers, amorphous versus graphitic particles.

Chapter 6
Conclusions and Future Work

6.1 Conclusions

Several carbonaceous nanomaterials, their novel methods of generation, and their performance as EDLC electrode materials have been presented in this work.

Through tight control of the operating parameters of an atmospheric plasma torch, we were able to synthesize amorphous and graphitic carbon nanoparticles from anthracene, mixtures of carbonaceous nanoparticles and graphitic sheets from hexane, and graphene from ethylene. These materials were formed from single-step syntheses (from precursor to end product), and had minimal surface groups. We were able to control the level of graphitization of each material by controlling parameters like the gas flow rates and the system pressures. Plasma synthesis techniques have yielded materials with unique characteristics unattainable by other methods.

A second, alternative method was developed by our group to produce graphene directly from graphite oxide and urea mixtures. It involved the expansion and reduction of the layers of graphite oxide as urea decomposes. The expansion-reduction mechanisms inherent to this process remove most oxygen surface groups while introducing nitrogen species to the graphene structure. Some of the advantages of using this new method of synthesis to

produce graphene include the low reaction temperatures and short reaction times. The expansion reduction process is also a dry process, thus there is no need for the use, and subsequent removal, of solvents or stabilizers required by colloidal methods. All of the required materials are inexpensive, safe, and abundant.

The carbonaceous materials (synthesized from the two methods) were assembled into electric double-layer capacitor test cells in an effort to correlate the microstructural properties of a carbonaceous nanomaterial to the material's capacitance:

We found that a high surface area was a necessary attribute for a nanomaterial to attain higher capacitance values. However, the capacitive performance of the graphitic nanoparticles and the graphene from expansion-reduction sythesis did not strictly follow this trend. The level of graphitization in the material seemed to enhance the capacitance of the graphitic nanoparticles. Similarly, the capacitance values of the graphene from expansion-reduction methods were improved by the level graphitization, and the nitrogen doping found in the samples. The correlation between a sample's graphitic nature and its performance as an electrode material was previously unreported. It was assumed that a crystalline long range order, like the one found in sheets of graphene, will have improved conductivity when compared to smaller, independent carbonaceous structures. In this work we successfully compared particles of similar sizes but different levels of crystallinity, and graphene in the

form of sheets and agglomerates. We found higher capacitance values and lower resistances for the crystalline particulates.

The nitrogen doping inherent to the expansion and reduction of graphite oxide and urea is a unique characteristic of the resultant graphene. This characteristic enhances the material's capacitive properties.

Analysis of the capacitance data led us to conclude that even though the most common way to report capacitive values for EDLC electrode material is in the form of μF/g or μF/cc, these values can at times be misleading. Perhaps a more comprehensive way to correlate the capacitance properties of carbonaceous electrode material would be to report the material's dielectric constant.

With the information obtained during this study, we have proven the capabilities of both synthetic methods (plasma, and expansion-reduction) for generating carbon electrode materials. Thus proving the validity of hypotheses 1 and 2. The evaluation of the materials' electrical properties has demonstrated which factors must be controlled to improve their feasibility as electrode materials in supercapacitors. Graphitic nanoparticles from plasma, and graphene from the expansion-reduction approach have shown the most promising characteristics. Consequently, we have also proven our third hypothesis.

6.2 Future Work

Currently, we are in the process of studying each materials response to capacitive cycling measurements. One of the next steps of this study will be to utilize sonication techniques to increase the surface area of the graphene material synthesized from the expansion-reduction method and conduct more extensive characterization of nitrogen groups.

Slight surface oxidation at low temperatures may increase surface area while maintaining the levels of graphitization in a sample, thus further improving EDLC performance. We plan to conduct these activation processes on the plasma-generated specimens. If surface activation is implemented, the effects of the oxidation processes on the surface functionalities will also need to be evaluated.

Appendix

Journal articles that resulted from this research

Wakeland S, Martinez R, Grey J, Luhrs CC (2010). "Production of graphene from graphite oxide using urea as expansion-reduction agent." Carbon **48**: 8.

Wakeland S, C. B., Luhrs CC (2010). Graphene, Graphitic And Amorphous Carbon Nanostructures Generation By Atmospheric Microwave Plasma Method. 37th Conference in Plasma Physics. E. Tatarova. Dublin, European Physical Society. EPS

Lambert T, Luhrs C, Chavez C, Wakeland S, Brumbach M, Alam Todd (2010). "Graphite Oxide As A Precursor For The Synthesis Of Disordered Graphenes Using The Aerosol-Through-Plasma Method." Carbon **48**: 9.

Conferences

Rio Grande Symposium on Advanced Materials: Oral presentation 2009
Wakeland S, Luhrs CC, Phillips J, Knapp A, Richard M. “Novel Sn/C Based Nanoparticle Architectures For Li Ion Battery Anodes.”

Rio Grande Symposium on Advanced Materials: Oral presentation 2010
Wakeland S, Martinez R, Majedi M, Carpenter B, Luhrs CC “Supercapacitor Electrode Materials Based on Graphene, Graphitic, and Amorphous Carbon Nanostructures”

MRS Fall 2010 Conference: Oral presentation
Wakeland S, Martinez R, Luhrs CC*. “Graphene Production from Graphite Oxide Using Urea an Expansion-reduction Agent”

References

1. Kotz R, C.M., *Principles and applications of electrochemical capacitors.* Electronchim Acta, 2000. **45**(15-16): p. 16.
2. Gamby J, T.P., Simon P, Fauvarque JF, Chesneau M, *Studies and characterisations of various activated carbons used for carbon/carbon supercapacitors.* Journal of Power Sources, 2001. **101**(1): p. 9.
3. Pandolfo AG, H.A., *Carbon properties and their role in supercapacitors.* Journal of Power Sources, 2006. **157**(1): p. 17.
4. Wakeland S, C.B., Luhrs CC, *Graphene, Graphitic And Amorphous Carbon Nanostructures Generation By Atmospheric Microwave Plasma Method*, in *37th Conference in Plasma Physics*, E. Tatarova, Editor. 2010, European Physical Society: Dublin.
5. Wakeland S, M.R., Grey J, Luhrs CC, *Production fo graphene from graphite oxide using urea as expansion-reduction agent.* Carbon, 2010. **48**: p. 8.
6. Hong WJ, B.H., Xu YX, Yao ZY, Gu ZZ, Shi GQ, *Preparation of gold nanoparticle/graphene composites with controlled weight contents and their application in biosensors.* Journal of Physical Chemistry C, 2010. **114**(4): p. 5.
7. Zhang YH, C.Y., Zhou KG, Liu CH, Zeng J, Zhang HL, et al., *Improving gas sensing properties of graphene by introducing dopants and defects: a first-principles study.* Nanotechnology, 2009. **20**(18): p. 8.
8. Schedin F, G.A., Morozov SV, Hill EW, Blake P, Katsnelson and e.a. MI, *Detection of individual gas molecules adsorbed on graphene.* Nature Materials, 2007. **6**(9): p. 4.
9. Frank IW, T.D., Van der Zande AM, McEuen PL., *Mechanical properties of suspended graphene sheets.* J Vac Sci Technol B, 2007. **25**(6): p. 4.
10. Cho D, L.S., Yang GM, Fukushima H, Drzal LT, *Dynamic mechanical and thermal properties of phenylethynylterminated polyimide composites reinforced with expanded graphite nanoplatelets.* Macromol Mater Eng, 2005. **290**(3): p. 10.
11. Ansari S, G.E., *Functionalized graphene sheetpoly(vinylidene fluoride) conductive nanocomposites.* J Polym Sci Pt B-Polym Phys, 2009. **47**(9): p. 10.
12. Stankovich S, D.D., Dommett GHB, Kohlhaas KM, Zimney EJ, Stach EA, *Graphene-based composite materials.* Nature, 2006. **442**(7100): p. 5.
13. Viculis LM, M.J., Mayer OM, Hahn HT, Kaner RB, *Intercalation and exfoliation routes to graphite nanoplatelets.* J Mater Chem, 2005. **15**(9): p. 5.
14. Lin Y M CH, J.K., Farmer DB, Avouris , Valde-Garcia A, *Dual-Gate Graphene FETs With f(T) of 50GHz.* IEEE Electron Device Letters, 2010. **31**(1): p. 3.
15. Li X, W.X., Zhang L, Lee S, Dai H., *Chemically derived, ultrasmooth graphene nanoribbon semiconductors.* Science, 2008. **319**: p. 4.
16. Burghard M, K.H., Kern K., *Carbon-based field-effect transistors for nanoelectronics.* Advanced materials, 2009. **21**(25-26): p. 15.

17. Berger C, S.Z., Li XB, Wu XS, Brown N, Naud C, et al., *Electronic confinement and coherence in patterned epitaxial graphene.* Science, 2006. **312**(5777): p. 6.
18. Stoller MD, P.S., Zhu YW, An JH, Ruoff RS, *Graphene-based ultracapacitors.* Nano Letters, 2008. **8**(10): p. 5.
19. Yong V, T.J., *Theoretical Efficiency of Nanostructured Graphene-Based Photovoltaics.* Small, 2010. **6**(2): p. 6.
20. Guo SJ, D.S., Wang EW, *Three-dimensional Pt-on-Pd bimetallic nanodendrites supported on graphene nanosheet: facile synthesis and used as an advanced nanoelectrocatalyst for methanol oxidation.* ACS Nano, 2010. **4**(1): p. 9.
21. Liu ZF, L.Q., Huang Y, Ma YF, Yin SG, Zhang XY, et al, *Organic Photovoltaic Devices Based on a Novel Acceptor Material: Graphene.* Advanced materials, 2008. **20**(20).
22. Liang MH, S.L., *Graphene-based electrode materials for rechargeable lithium batteries.* Journal of Material Chemistry, 2009. **19**(33): p. 8.
23. H, S., *Activated carbons and double layer capacitance.* Electronchim Acta, 1996. **41**(10): p. 7.
24. Qu DY, S.H., *1998.* Journal of Power Sources, Studies of activated carbons used in double-layer capacitors. **74**(1): p. 12.
25. Frackowiak E, B.F., *Electrochemical storage of energy in carbon nanotubes and nanostructured carbons.* Carbon, 2002. **40**(10): p. 13.
26. Wei DC, L.Y., Wang Y, Zhang HL, Huang LP, Yu G., *Synthesis of N-doped graphene by chemical vapor deposition and its electrical properties.* Nano Letters, 2009. **9**(5): p. 7.
27. Dato A RV, L.Z., Phillips J, Frenklach M, *Substrate-free gas-phase synthesis of graphene sheets.* Nano Letters, 2008. **8**(7): p. 5.
28. Schniepp HC LJ, M.M., Sai H, Herrera-Alonso M, Adamson DH, et al, *Functionalized Single Graphene Sheets Derived from Splitting Graphite Oxide.* Journal of Physical Chemistry B Letters, 2006. **110**: p. 5.
29. McAllister MJ LJ, A.D., Schniepp HC, Abdala AA, Liu J, et al, *Single sheet functionalized Graphene by Oxidation and Thermal Expansion of Graphite.* Chem Mater, 2007. **19**: p. 9.
30. Gass MH BU, B.A., Wang P, Nair RR, Geim AK, *Free-standing graphene at atomic resolution.* Nature Nanotechnology, 2008. **3**(11): p. 6.
31. Ju HM, H.S., Choi SH, Lee HL, *Structures of thermally and chemically reduced graphene.* Material Letters, 2010. **64**(3): p. 4.
32. Stankovich S, D.D., Piner R, Kohlhaas KA, Kleinhammes A, Jia Y, et al., *Synthesis of Graphene-based Nanosheets Via Chemical Reduction fo Exfoliated Graphite Oxide.* Carbon, 2007. **45**: p. 7.
33. HO, P., *Handbook of carbon, graphite diamond and fullerenes*. 1993: Noyes Publications.
34. Liberman MA, L.A., *Principles of Plasma Discharges and Materials Processing*. 2 ed. 1994: Wiley-Interscience.
35. Chun-Ku C, P.W., Phillips Jonathan, *Plasma Torch Production of Macroscopic Carbon Nanotube Structures.* Carbon, 2003. **41**.
36. Dato A, R.V., Lee Z, Phillips J, Frencklach M, Nano Letters, 2008. **8**(2012).

37. Jenkins GM, K.K., *Polymeric carbons*. 1976, Cambridge: Cambridege University Press.
38. Liming Y, K.S., Wenchong H, Zhi C, *Ethylene flame synthesis of well-aligned multi-walled carbon nanotubes.* Chemical Physics Letters, 2001. **346**(1-2): p. 6.
39. Hernadi K, F., Nagy JB, Siska A, Kiricsi I, *Production of nanotubes by the ctalytic decompostion of different carbon-containing compounds.* Applied Catalysis A, 2000. **199**(2): p. 11.
40. Atwater, M.A., et al., *The production of carbon nanofibers and thin films on palladium catalysts from ethylene-oxygen mixtures.* Carbon, 2009. **47**(9): p. 2269-2280.
41. Rez P, M.D., *The Theory and Interpretation of Electron Energy Loss Near-Edge fine Structure.* Annu. Rev. Mater. Res., 2008. **38**: p. 24.
42. Dreyer DR, P.S., Bielawski CW, Ruoff RS, *The chemistry of graphene oxide.* Chem Soc Rev, 2010. **39**(1): p. 13.
43. Jung I, D.D., Park S, Cai W, Mielke SL, Ruoff RS., *Effect of water vapor on electrical properties of individual reduced graphene oxide sheets.* J Phys Chem C, 2008. **112**(51): p. 5.
44. Stankovich S PR, C.X., Wu NQ, Nguyen ST, Ruoff RS, *Stable aqueous dispersions of graphitic nanoplatelets via the reduction of exfoliated graphite oxide in the presence of poly(sodium 4-styrenesulfonate).* Journal of Material Chemistry, 2006. **16**(2): p. 4.
45. Wang GX, Y.J., Park J, Gou XL, Wang B, Liu H, et al., *Facile synthesis and characterization of graphene nanosheets.* J Phys Chem C, 2008. **112**(22): p. 4.
46. Hummers WS, O.R., *Preparation of graphitic oxide.* J Am Chem Soc, 1958. **80**(6).
47. Schaber PM, C.J., Higgins S, Dietz E, Thielen D, Anspach B, et al., *Study of the urea thermal decomposition (pyrolysis) reaction and importance to cyanuric acid production.* Am Lab, 1999. **31**(16): p. 9.
48. AM., W., *The thermal-decomposition of urea – an undergraduate thermal-analysis experiment.* J Chem Educ, 1987. **64**(2): p. 3.
49. Graf D, M.F., Ensslin K, Stampfer C, Jungen A, Hierold C, et al., *Spatially resolved Raman spectroscopy of single- and few-layer graphene.* Nano Letters, 2007. **7**(2): p. 5.
50. Yan J, H.E., Kim P, Pinczuk A., *Observation of anomalous phonon softening in bilayer graphene.* Phys Rev Lett, 2008. **101**(13).
51. Muller JO, A.P., Smarsly B, Su DS, Antonietti M., *TEM/EELS/XRD investigation of the graphitization process in carbonaceous materials.* Microsc Microanal, 2007. **13**.
52. Fang HL, D.H., *Urea thermolysis and NOx reduction with and without SCR catalysts.* Appl Catal B – Environ, 2003. **46**(1): p. 18.
53. Koebel M, S.E., *Thermal and hydrolytic decomposition of urea for automotive selective catalytic reduction systems: thermochemical and practical aspects.* Ind Eng Chem Res, 2003. **42**(10): p. 8.
54. Yim SD, K.S., Baik JH, Nam IS, Mok YS, Lee JH, et al., *Decomposition of urea into NH3 for the SCR process.* Ind Eng Chem Res, 2004. **43**(16): p. 8.

55. Phillips J, L.C., Leseman Z, Zea HR., *Metal compound reduction mediated by nitrogen–hydrogen containing molecules: generation of metal and alloy nanoparticles in simple rapid process.* 2010: USA.
56. Schaber PA, C.J., Higgins S, Thielen D, Anspach B, Brauer J., *Thermal decomposition (pyrolysis of urea in an open reaction vessel.* Thermochim Acta, 2004. **424**(1-2): p. 12.
57. Wynne AM, *The thermal-decomposition of urea – an undergraduate thermal-analysis experiment.* J Chem Educ, 1987. **64**(2): p. 3.
58. Slabaugh WH, S.B.I.o.a.w.g.o., *Interactions of ammonia with graphite oxide.* j phys Chem, 1962. **66**(3): p. 6.
59. Brunauer S, E.P.H., Teller E, *Adsorption of Gases in Multimolecular Layers.* Journal of American Chemistry, 1938. **60**(2): p. 11.
60. Conway B.E., Journal of Solid State Chemistry, 2003. **637**(7).
61. Inakagi M, R.L.R., Carbon, 2002. **40**.
62. Marsh H., *Introduction to Carbon Science*. 1989: Butterworths.
63. Bourrat X, M.H., Rodriquez-Reynoso,, *Science of Carbon Materials*. 2000: Universidad de Alicante.
64. Biniak, P., *Chemsitry and Physics of Carbon*. Vol. 27. 2001, New York: Marcel Dekker.
65. Panchakarla L.S., S.K.S., Saha S.K., Govindaraj A., Krishnamurthy H.R., Waghmare U.V., Rao C.N.R.,, *Synthesis, Sructure, and Properties of Boron- and Nitrogen-Doped Graphene.* Advanced Materials, 2009. **21**: p. 5.
66. Morimoto, S., Journal of Power Sources, 1996. **60**.
67. Wang X, L.X., Zhang Y, Weber P, Wang H, Guo J, Dai H, *N-Doping Of Graphene Through Electrothermal Reactions With Ammonia.* Science, 2009. **324**: p. 4.